Supplementary Materials for

Spin-group symmetry in magnetic materials with negligible spin-orbit coupling

Pengfei Liu[1,2], Jiayu Li[1], Jingzhi Han[2], Xiangang Wan[3,*] and Qihang Liu[1,4,5,*]

[1]*Shenzhen Institute for Quantum Science and Engineering and Department of Physics, Southern University of Science and Technology, Shenzhen 518055, China*

[2]*School of Physics, Peking University, Beijing 100871, People's Republic of China*

[3]*National Laboratory of Solid State Microstructures and School of Physics, Nanjing University, Nanjing 210093, China and Collaborative Innovation Center of Advanced Microstructures, Nanjing University, Nanjing 210093, China*

[4]*Guangdong Provincial Key Laboratory of Computational Science and Material Design, Southern University of Science and Technology, Shenzhen 518055, China*

[5]*Shenzhen Key Laboratory of for Advanced Quantum Functional Materials and Devices, Southern University of Science and Technology, Shenzhen 518055, China*

[*]Emails: xgwan@nju.edu.cn; liuqh@sustech.edu.cn

Contents

SOME OF THE NOTATIONS

G_0 A group that is either point group or space group

G_{0p} Point group (PG)

G_{0s} Space group (SG)

$O^s(3)$ Orthogonal group of spin symmetries (OS)

G_{SP} Spin point group (SPG)

G_{SS} Spin space group (SSG)

G_{SO} Spin-only group

G_{SOP} Spin-only point group

G_{NS} Nontrivial spin group

G_{NSP} Nontrivial spin point group

G^s_{NSP} Spin rotation part of a nontrivial spin point group

I. PRELIMINARIES ABOUT PRODUCT OF GROUPS

A. External direct product of two groups

For both A and B being groups, with binary operations denoted as $*$ and $\circ$, then the external direct product of A and B is defined as a new group:

$$A \otimes B = \{(a, b) |\, a \in A, b \in B\}, \tag{S1}$$

with binary operation $(a, b) \times \left(a', b'\right) = (a * a, b \circ b)$. The external direct product defined here is the direct product defined in general textbooks [1].

B. Product of two subsets of a group

Assuming A and B are two subsets of group G with multiplication $*$, then the product of A and B is defined as:

$$AB = \{a * b |\ a \in A, b \in B\}\ (or\ for\ simplicity, AB = \{ab |\ a \in A, b \in B\}) \quad \text{(S2)}$$

The product of A and B is a subset of G. However, even if both A and B are groups, AB is not necessarily a subgroup of G. Assuming both A and B are subgroups of G, then AB is a subgroup of G if and only if $AB = BA$.

C. Internal semidirect product

Assuming both A and B are subgroups of G with a trivial intersection, i.e., $A \cap B = \{E\}$ with E representing the identity element in group G, and AB is also a subgroup of G. AB is called the internal Zappa-Szep product of A and B. In this case, if either A or B is a normal subgroup of AB, then the product AB is defined as an internal semidirect product of A and B, denoted as $A \rtimes B$ (if A is a normal subgroup of AB) or $A \ltimes B$ (if B is a normal subgroup of AB).

D. Internal direct product of two subgroups of group G

Assuming AB is the internal Zappa-Szep product of A and B, with A and B being subgroups of G with $A \cap B = \{E\}$, and both A and B are normal subgroups of AB, then the product AB is defined as an internal direct product of A and B, denoted as $A \times B$.

It is easy to show that if both A and B are normal subgroups of AB, then all elements in A commute with all elements in B, i.e., $ab = ba$ for all $a \in A$ and all $b \in B$. Thus, the internal direct product of A and B is isomorphic to the external direct product of A and B, i.e.,

$$A \times B = \{a * b |\ a \in A, b \in B\} \cong A \otimes B. \tag{S3}$$

II. SYMMETRY OF GENERAL SINGLE-ELECTRON HAMILTONIANS

A. Definition of symmetry operators

To define spatial and spin symmetry operators, we first recall the definition of position, momentum, and spin operators. The position and momentum operators are denoted as $\hat{\boldsymbol{r}} = \left(\hat{r}_x, \hat{r}_y, \hat{r}_z\right)^T$ and $\hat{\boldsymbol{p}} = \left(\hat{p}_x, \hat{p}_y, \hat{p}_z\right)^T$, satisfying $\left[\hat{r}_i, \hat{r}_j\right] = 0, \left[\hat{p}_i, \hat{p}_j\right] = 0, \left[\hat{r}_i, \hat{p}_j\right] = i\hbar$, with their eigenstates $|\boldsymbol{r}'\rangle$, $|\boldsymbol{p}'\rangle$ satisfying $\hat{\boldsymbol{r}}|\boldsymbol{r}'\rangle = \boldsymbol{r}'|\boldsymbol{r}'\rangle$ and $\hat{\boldsymbol{p}}|\boldsymbol{p}'\rangle = \boldsymbol{p}'|\boldsymbol{p}'\rangle$, respectively. Then, we can write the position and momentum operator as $\hat{\boldsymbol{r}} = \int \boldsymbol{r}'|\boldsymbol{r}'\rangle\langle\boldsymbol{r}'|d\boldsymbol{r}'$ and $\hat{\boldsymbol{p}} = \int \boldsymbol{p}'|\boldsymbol{p}'\rangle\langle\boldsymbol{p}'|d\boldsymbol{p}'$. The spin operator is denoted as $\hat{\boldsymbol{\sigma}} = \left(\hat{\sigma}_x, \hat{\sigma}_y, \hat{\sigma}_z\right)^T$ with three components satisfying $[\hat{\sigma}_i, \hat{\sigma}_j] = i\hbar\varepsilon_{ijk}\hat{\sigma}_k$. The eigenstates could be written as $|s, m_i\rangle$, with $\hat{\sigma}_i|s, m_i\rangle = \hbar m_i|s, m_i\rangle$ and $\hat{\boldsymbol{\sigma}}^2\ |s, m_i\rangle = (\hat{\sigma}_x{}^2 + \hat{\sigma}_y{}^2 + \hat{\sigma}_z{}^2)|s, m_i\rangle = s(s+1)\hbar^2|s, m_i\rangle$. Since spin and spatial degrees of freedom are independent of each other, we have $\left[\hat{\sigma}_i, \hat{r}_j\right] = 0$ and $\left[\hat{\sigma}_i, \hat{p}_j\right] = 0$.

We define the spatial inversion, rotation, and translation operator as follows.

$$\hat{I}|\boldsymbol{r}'\rangle = |-\boldsymbol{r}'\rangle, \tag{S4}$$

$$\widehat{C_{\boldsymbol{n}}(\theta)}|\boldsymbol{r}'\rangle = |R_{\boldsymbol{n}}(\theta)\boldsymbol{r}'\rangle, \tag{S5}$$

$$\hat{\tau}_{\boldsymbol{t}}|\boldsymbol{r}'\rangle = |\boldsymbol{r}' + \boldsymbol{t}\rangle. \tag{S6}$$

Then, $\{\widehat{g|\tau_{\boldsymbol{t}}}\}$ is represented by $\hat{\tau}_{\boldsymbol{t}}\hat{g}$. Thus, a quantum state $|\psi(\boldsymbol{r})\rangle = \int \psi(\boldsymbol{r}')|\boldsymbol{r}'\rangle d\boldsymbol{r}'$ is transformed by $\{\widehat{g|\tau_{\boldsymbol{t}}}\}$ as:

$$\widehat{\tau_t}\hat{g}|\psi(\boldsymbol{r})\rangle = |\psi(R(g)^{-1}\boldsymbol{r} - R(g)^{-1}\boldsymbol{t})\rangle. \tag{S7}$$

Furthermore, we can show that:

$$\widehat{\{g|\tau_t\}}\hat{\boldsymbol{r}}\widehat{\{g|\tau_t\}}^{-1} = R(g)^{-1}\left(\widehat{r_x - t_x}, \widehat{r_y - t_y}, \widehat{r_z - t_z}\right)^T = R(g)^{-1}\widehat{\boldsymbol{r} - \boldsymbol{t}}, \tag{S8}$$

with

$$\widehat{r_i - t_i} \equiv \int (r'_i - t_i)|\boldsymbol{r}'\rangle\langle\boldsymbol{r}'|d\boldsymbol{r}', \tag{S9}$$

$$\widehat{\boldsymbol{r} - \boldsymbol{t}} \equiv \int (\boldsymbol{r}' - \boldsymbol{t})|\boldsymbol{r}'\rangle\langle\boldsymbol{r}'|d\boldsymbol{r}'. \tag{S10}$$

Similarly, we have

$$\widehat{\{g|\tau_t\}}\hat{\boldsymbol{p}}\widehat{\{g|\tau_t\}}^{-1} = R(g)\hat{\boldsymbol{p}}. \tag{S11}$$

$$\widehat{\{g|\tau_t\}}\hat{\boldsymbol{\sigma}}\widehat{\{g|\tau_t\}}^{-1} = \hat{\boldsymbol{\sigma}}. \tag{S12}$$

We define the spin-rotation operator as follows:

$$\widehat{U_{\boldsymbol{n}}(\omega)}\hat{\boldsymbol{\sigma}}\widehat{U_{\boldsymbol{n}}(\omega)}^{-1} = R_{\boldsymbol{n}}(\omega)^{-1}\hat{\boldsymbol{\sigma}}. \tag{S13}$$

Since the spin operator and position operator commute with each other, we have

$$\widehat{U_{\boldsymbol{n}}(\omega)}\hat{\boldsymbol{r}}\widehat{U_{\boldsymbol{n}}(\omega)}^{-1} = \hat{\boldsymbol{r}}, \tag{S14}$$

$$\widehat{U_{\boldsymbol{n}}(\omega)}\hat{\boldsymbol{p}}\widehat{U_{\boldsymbol{n}}(\omega)}^{-1} = \hat{\boldsymbol{p}}, \tag{S15}$$

where

$$\widehat{U_{\boldsymbol{n}}(\omega)} = exp(-i\omega\tfrac{\boldsymbol{n}\cdot\hat{\boldsymbol{\sigma}}}{\hbar}). \tag{S16}$$

Additionally, we can easily show that $\sum_j R_{\boldsymbol{n}}(\omega)^{-1}{}_{ij}\hat{\sigma}_j\,\widehat{U_{\boldsymbol{n}}(\omega)}|s, m_i\rangle = \hbar m_i\widehat{U_{\boldsymbol{n}}(\omega)}|s, m_i\rangle$.

The operation that could inverse spin is realized by the time-reversal operator, which satisfies the following relations:

$$\hat{T}\hat{\boldsymbol{r}}\hat{T}^{-1} = \hat{\boldsymbol{r}}, \tag{S17}$$

$$\hat{T}\hat{\boldsymbol{p}}\hat{T}^{-1} = -\hat{\boldsymbol{p}}, \tag{S18}$$

$$\widehat{T}\widehat{\boldsymbol{\sigma}}\widehat{T}^{-1} = -\widehat{\boldsymbol{\sigma}}. \tag{S19}$$

Therefore, the kinetic energy term $\frac{\widehat{\boldsymbol{p}}^2}{2m}$ and spin-orbit coupling term $\frac{1}{2m^2c^2}(\nabla V(\widehat{\boldsymbol{r}}) \times \widehat{\boldsymbol{p}}) \cdot \widehat{\boldsymbol{\sigma}}$ are both invariant under $\widehat{T}$, because the former is proportional to $\widehat{\boldsymbol{p}}^2$, and the latter is proportional to $\widehat{\boldsymbol{p}} \times \widehat{\boldsymbol{\sigma}}$, and thus also invariant under $\widehat{T}$. Furthermore, $\widehat{T}$ and $\widehat{U_{\boldsymbol{n}}(\omega)}$ commute with each other, and they commute with spatial translation, spatial rotation, and spatial inversion operators.

Thus, spin symmetry operators and spatial symmetry operators composing a spin group symmetry operator are commutable:

$$\{\widehat{g_s||g|\tau_{\boldsymbol{t}}}\} = \widehat{g}_s\widehat{\tau}_{\boldsymbol{t}}\widehat{g} = \widehat{\tau}_{\boldsymbol{t}}\widehat{g}\widehat{g}_s. \tag{S20}$$

B. Symmetry constraint of the general single-electron Hamiltonian

The single-electron Hamiltonian with both spin-orbit coupling (SOC) and magnetic order could be written as:

$$\widehat{H} = \frac{\widehat{\boldsymbol{p}}^2}{2m} + V(\widehat{\boldsymbol{r}}) + \frac{1}{2m^2c^2}(\nabla V(\widehat{\boldsymbol{r}}) \times \widehat{\boldsymbol{p}}) \cdot \widehat{\boldsymbol{\sigma}} + \boldsymbol{S}(\widehat{\boldsymbol{r}}) \cdot \widehat{\boldsymbol{\sigma}}, \tag{S21}$$

Such Hamiltonian is invariant under certain symmetry operations, i.e., $\widehat{g}\widehat{H}\widehat{g}^{-1} = \widehat{H}$, which form the full symmetry group of the Hamiltonian. We next discuss the symmetry constraint of the four terms separately. First, it is obvious that the kinetic energy term $\frac{\widehat{\boldsymbol{p}}^2}{2m}$ imposes no constraint on the symmetry of Hamiltonian. Second, while any spin symmetry operations leave $V(\widehat{\boldsymbol{r}})$ invariant, the constraint of $V(\widehat{\boldsymbol{r}})$ by spatial operations satisfies:

$$\{\widehat{E||g|t}\}V(\widehat{\boldsymbol{r}})\{\widehat{E||g|t}\}^{-1} = V\big(R(g)^{-1}\widehat{\boldsymbol{r}-\boldsymbol{t}}\big) = V(\widehat{\boldsymbol{r}}), \tag{S22}$$

The spin-orbit coupling term $\frac{1}{2m^2c^2}(\nabla V(\widehat{\boldsymbol{r}}) \times \widehat{\boldsymbol{p}}) \cdot \widehat{\boldsymbol{\sigma}}$ involves both spin and spatial

degrees of freedom. Because it is dependent on $V(\hat{\boldsymbol{r}})$, we only consider symmetry operations that keep $V(\hat{\boldsymbol{r}})$ invariant. It is easy to see that $\frac{1}{2m^2c^2}(\nabla V(\hat{\boldsymbol{r}}) \times \hat{\boldsymbol{p}}) \cdot \hat{\boldsymbol{\sigma}}$ is invariant under spatial inversion, spatial translation, and time-reversal symmetries. For spatial and spin rotations, we have

$$\begin{aligned}
&\widehat{C_{\boldsymbol{n}}(\theta)}\left(\frac{1}{2m^2c^2}(\nabla V(\hat{\boldsymbol{r}}) \times \hat{\boldsymbol{p}}) \cdot \hat{\boldsymbol{\sigma}}\right)\widehat{C_{\boldsymbol{n}}(\theta)}^{-1} \\
&= \frac{1}{2m^2c^2}\left(R_{\boldsymbol{n}}(\theta)\nabla V(R_{\boldsymbol{n}}(\theta)^{-1}\hat{\boldsymbol{r}}) \times R_{\boldsymbol{n}}(\theta)\hat{\boldsymbol{p}}\right) \cdot \hat{\boldsymbol{\sigma}} \\
&= \frac{1}{2m^2c^2}R_{\boldsymbol{n}}(\theta)(\nabla V(\hat{\boldsymbol{r}}) \times \hat{\boldsymbol{p}}) \cdot \hat{\boldsymbol{\sigma}}. \qquad \text{(S23)}
\end{aligned}$$

$$\begin{aligned}
&\widehat{U_{\boldsymbol{n}}(\omega)}\left(\frac{1}{2m^2c^2}(\nabla V(\hat{\boldsymbol{r}}) \times \hat{\boldsymbol{p}}) \cdot \hat{\boldsymbol{\sigma}}\right)\widehat{U_{\boldsymbol{n}}(\omega)}^{-1} \\
&= \frac{1}{2m^2c^2}(\nabla V(\hat{\boldsymbol{r}}) \times \hat{\boldsymbol{p}}) \cdot \widehat{U_{\boldsymbol{n}}(\omega)}\hat{\boldsymbol{\sigma}}\widehat{U_{\boldsymbol{n}}(\omega)}^{-1} \\
&= \frac{1}{2m^2c^2}(\nabla V(\hat{\boldsymbol{r}}) \times \hat{\boldsymbol{p}}) \cdot R_{\boldsymbol{n}}(\theta)\hat{\boldsymbol{\sigma}}. \qquad \text{(S24)}
\end{aligned}$$

From Eq. (S27) and (S28), a symmetry operation that keeps the spin-orbit coupling term invariant has two possible forms: 1) containing neither spin rotation nor spatial rotation, e.g., spatial inversion and time-reversal; 2) containing a spin rotation and a spatial rotation with the same rotation axis and same rotation angle, i.e., $U_{\boldsymbol{n}}(\theta)C_{\boldsymbol{n}}(\theta)$.

Like the SOC term, the magnetic term $\boldsymbol{S}(\hat{\boldsymbol{r}}) \cdot \hat{\boldsymbol{\sigma}}$ also contains both spin and spatial degrees of freedom, and thus constrains spin and spatial symmetry simultaneously. We note that, since we are considering single-electron systems, the spin rotation operator and time-reversal operator directly act on $\hat{\boldsymbol{\sigma}}$, while the local spin arrangements are represented by the exchange field $\boldsymbol{S}(\hat{\boldsymbol{r}})$. Nevertheless, the action of spin group operator, including spatial and spin operations, on this term can be fully taken as the action on $\boldsymbol{S}(\hat{\boldsymbol{r}})$. From Eq. (S8) and (S12-14), we have

$$\widehat{\{g|\tau_{\boldsymbol{t}}\}}\boldsymbol{S}(\hat{\boldsymbol{r}}) \cdot \hat{\boldsymbol{\sigma}}\widehat{\{g|\tau_{\boldsymbol{t}}\}}^{-1} = \boldsymbol{S}(R(g)^{-1}\widehat{\boldsymbol{r}-\boldsymbol{t}}) \cdot \hat{\boldsymbol{\sigma}}. \qquad \text{(S25)}$$

$$\widehat{U_n(\theta)}\boldsymbol{S}(\hat{\boldsymbol{r}})\cdot\hat{\boldsymbol{\sigma}}\widehat{U_n(\theta)}^{-1}=\boldsymbol{S}(\hat{\boldsymbol{r}})\cdot R_{\boldsymbol{n}}(\theta)^{-1}\hat{\boldsymbol{\sigma}}=R_{\boldsymbol{n}}(\theta)\boldsymbol{S}(\hat{\boldsymbol{r}})\cdot\hat{\boldsymbol{\sigma}}. \tag{S26}$$

$$\hat{T}J\boldsymbol{S}(\hat{\boldsymbol{r}})\cdot\hat{\boldsymbol{\sigma}}\hat{T}^{-1}=\boldsymbol{S}(\hat{\boldsymbol{r}})\cdot\hat{T}\hat{\boldsymbol{\sigma}}\hat{T}^{-1}=\boldsymbol{S}(\hat{\boldsymbol{r}})\cdot(-\hat{\boldsymbol{\sigma}})=(-\boldsymbol{S}(\hat{\boldsymbol{r}}))\cdot\hat{\boldsymbol{\sigma}}. \tag{S27}$$

Thus, the action of spin group operator $\{g_s\widehat{||g|}\tau_{\boldsymbol{t}}\}$ on the magnetic term gives rise to the action on the exchange field $\boldsymbol{S}(\hat{\boldsymbol{r}})$ with the form $R(g_s)\boldsymbol{S}(R(g^{-\mathbf{1}})(\widehat{\boldsymbol{r}-\boldsymbol{t}}))$, which is identical to the action of spin group symmetry operation on spin arrangement defined in Eq. (A19).

C. Symmetry of nonmagnetic single-electron Hamiltonian

Without external magnetic field, magnetic order, or spin-orbit coupling, the single-electron Hamiltonian simply has the form:

$$\hat{H}=\frac{\hat{\boldsymbol{p}}^2}{2m}+V(\hat{\boldsymbol{r}}). \tag{S28}$$

Apparently, spatial symmetry of such type of Hamiltonian is described by space groups (point groups) denoted by G_0, while the spin symmetry operations are completely unbroken and form an orthogonal group $O^s(3)$ (defined in (A1)). Then, the whole symmetry group of this Hamiltonian is:

$$G_0\otimes O^s(3). \tag{S29}$$

In the conventional treatment of such type of Hamiltonian, the spin degrees of freedom are usually neglected because the Hamiltonian contains no spin operator. In this way, the symmetry group of the Hamiltonian is of the form $G_0\otimes Z_2^K$ where $Z_2^K=\{E,K\}$, with K being the spinless time-reversal operator satisfying $K^2=1$. In contrast, the treatment of spin group also includes K as the combined operation of a spin rotation operation with rotation angle π and a spin-1/2 time-reversal operation, i.e., $\{U_{\boldsymbol{n}}(\pi)T||E|0\}$, which satisfies $\{U_{\boldsymbol{n}}(\pi)T||E|0\}^2=1$.

If we add spin-orbit coupling (SOC) in addition to the above Hamiltonian, the resulting Hamiltonian is of the following form:

$$\widehat{H} = \frac{\widehat{\boldsymbol{p}}^2}{2m} + V(\widehat{\boldsymbol{r}}) + \frac{1}{2m^2c^2}(\nabla V(\widehat{\boldsymbol{r}}) \times \widehat{\boldsymbol{p}}) \cdot \widehat{\boldsymbol{\sigma}}. \tag{S30}$$

Then, from the analysis in section B, spin rotation and spatial rotation must be exerted synchronously, i.e., they must be exerted with the same rotation angle and the same rotation axis so that the SOC term is invariant. From the perspective of symmetry group, the symmetry group is reduced from the group $G_0 \otimes O^s(3)$ to one of its subgroups. If we write G_0 as:

$$G_0 = \{C_{\boldsymbol{n}_1}(\theta_1)I^{b_1}|t_1\}Q + \ldots + \{C_{\boldsymbol{n}_a}(\theta_a)I^{b_a}|t_a\}Q, \tag{S31}$$

where Q is the translation group of Bravais lattice, then the symmetry group of the Hamiltonian with SOC term is:

$$G \otimes Z_2^T, \tag{S32}$$

where G is the group that is formed from G_0 by adding every element of G_0 with a spin rotation that has the same rotation axis and the same rotation angle as the spatial rotation, and Z_2^T is the group generated from time-reversal symmetry:

$$G = \{U_{\boldsymbol{n}_1}(\theta_1)||C_{\boldsymbol{n}_1}(\theta_1)I^{b_1}|t_1\}Q + \ldots + \{U_{\boldsymbol{n}_a}(\theta_1)||C_{\boldsymbol{n}_a}(\theta_a)I^{b_a}|t_a\}Q, \tag{S33}$$

$$Z_2^T = \{\{E||E|0\}, \{T||E|0\}\}. \tag{S34}$$

It is obvious that the group G is isomorphic to point/space group G_0 because spin rotation is locked to the spatial rotation and thus not revealed in symmetry analysis. Then, space group is enough to describe the system's symmetry with SOC without magnetic order. Furthermore, since the representations of spin rotation with the basis of spin ½ states is projective, which have rotation of 2π give rise to a minus identity matrix, it is conventional to consider a kind of enhanced group called double group, which could be

written as $G^d = G \cup 1^d G$, where 1^d represents the spatial rotation of 2π, and find all of the representations of G^d that satisfy representation matrix of 1^d being minus identity, so that the energy level degeneracy of spin-orbit coupled system could be described [2,3].

D. Symmetry of magnetic single-electron Hamiltonian

From the Hamiltonian with spin-orbit coupling, we introduce magnetic order by adding a term $H_{mag} = \boldsymbol{S}(\hat{\boldsymbol{r}}) \cdot \hat{\boldsymbol{\sigma}}$:

$$\hat{H} = \frac{\hat{\boldsymbol{p}}^2}{2m} + V(\hat{\boldsymbol{r}}) + \frac{1}{2m^2c^2}(\nabla V(\hat{\boldsymbol{r}}) \times \hat{\boldsymbol{p}}) \cdot \hat{\boldsymbol{\sigma}} + \boldsymbol{S}(\hat{\boldsymbol{r}}) \cdot \hat{\boldsymbol{\sigma}}. \tag{S35}$$

Because of the magnetic term, it has been shown that certain spatial symmetry and spin symmetry could be broken. Furthermore, because the SOC term still exists, spin and spatial rotation must be performed synchronously. Thus, symmetry group with one type of rotation is enough to describe symmetry of the Hamiltonian. Then, if the Hamiltonian corresponds to a periodic crystal, the symmetry of this Hamiltonian should be described by one of the 1651 magnetic space groups, except grey groups, denoted as G_m. For describing spin ½ particles, magnetic double space group, defined as $G_m^d = G_m \cup 1^d G_m$, is conventionally used, like double space group in nonmagnetic systems.

We now focus on the Hamiltonian without spin-orbit coupling but with magnetic order:

$$\hat{H} = \frac{\hat{\boldsymbol{p}}^2}{2m} + V(\hat{\boldsymbol{r}}) + \boldsymbol{S}(\hat{\boldsymbol{r}}) \cdot \hat{\boldsymbol{\sigma}}. \tag{S36}$$

Because of the absence of spin-orbit coupling, no restriction forces the spatial and spin rotation to be exerted synchronously. However, the magnetic term $\boldsymbol{S}(\hat{\boldsymbol{r}}) \cdot \hat{\boldsymbol{\sigma}}$ could restrict spin and spatial symmetry in a way identical to the restriction of spin arrangement on spin group symmetry, as shown in Section B. Thus, this term may partially lock spatial

rotation and spin rotation symmetry, making it necessary to consider the spin rotation and spatial rotation separately. We could have elements of the form $\{T^q U_{\boldsymbol{m}}(\varphi)||C_{\boldsymbol{n}}(\theta)I^w|\tau_{\boldsymbol{t}}\}$, where m and n are not necessarily parallel axes and φ and θ are not necessarily the same angle. For instance, in a ferromagnetic system, pure spatial rotation could be allowed by the magnetic term. In a noncollinear magnetic system, the operation with φ being an integral multiple of θ could be allowed (exemplified in section IV). Then the full symmetry properties of single-electron Hamiltonian are described by spin groups, while magnetic groups are not capable.

III. SYMMETRY OF A TIGHT-BINDING HAMILTONIAN OF HEXAGONAL MOLECULE

We first use a tight-binding Hamiltonian of a hexagonal molecule with 6 sites equipped with in-plane local magnetic moments at all sites and one orbital per site (see Fig. S1(a)) to show that SPG symmetry could emerge in the absence of SOC. We neglect spatial inversion symmetry for simplicity and assume the symmetry group without local magnetic moments is $D_6 \otimes O^s(3)$. With spin arrangements, the spatial rotations $C_{\boldsymbol{z}}(\frac{\pi}{3})$ and $C_{\boldsymbol{x}}(\pi)$ are generally broken viewed from the symmetry of the magnetic group. However, from the point of view of spin group, the symmetry operations that are combinations of $C_{\boldsymbol{z}}(\frac{\pi}{3})$ / $C_{\boldsymbol{x}}(\pi)$ and spin rotations could be preserved so that the corresponding nontrivial spin group is isomorphic to D_6. To validate such peculiar spin group symmetry, we assume that all of the six local magnetic moments have the same magnitude but point randomly within the x-y plane $\boldsymbol{S}_i = S[Cos(\phi_i), Sin(\phi_i), 0]$, then find

all of the magnetic orders that have $\{U_{\boldsymbol{m}}(\varphi)||C_{\boldsymbol{z}}(\frac{\pi}{3})\}$ and $\{U_{\boldsymbol{n}}(\theta)||C_{\boldsymbol{x}}(\pi)\}$ symmetry.

We use a basis with local spin quantization axes directing along the local magnetic moments ($\boldsymbol{z}_i = [Cos(\phi_i), Sin(\phi_i), 0]\ i = 1, \ldots, 6$), denote the eigenstates of spin operator along $\boldsymbol{z}_i$ direction as $|i, \boldsymbol{z}_i \cdot \boldsymbol{\sigma} = \alpha\rangle$, and assume nearest-neighbor hopping between different sites. Then the matrix elements of the tight-binding Hamiltonian are of the following form, which is a function of the relative angle between spin axes of two neighbor sites:

$$\langle i, \boldsymbol{z}_i \cdot \boldsymbol{\sigma} = \alpha|\widehat{H}|j, \boldsymbol{z}_j \cdot \boldsymbol{\sigma} = \beta\rangle = t\left[\delta_{i,j+1} + \delta_{i,j-1}\right]X\left(\phi_i - \phi_j\right)_{\alpha\beta} + \delta_{i,j}(S\sigma_z)_{\alpha\beta}, \quad \text{(S37)}$$

where $X\left(\phi_i - \phi_j\right)$ is the matrix representing the spin rotation between two neighbor spin quantization axes with the form:

$$X(\theta) \equiv \begin{bmatrix} Cos\left(\frac{\theta}{2}\right) & i\,Sin\left(\frac{\theta}{2}\right) \\ i\,Sin\left(\frac{\theta}{2}\right) & Cos\left(\frac{\theta}{2}\right) \end{bmatrix}. \quad \text{(S38)}$$

Then, the symmetry operations $\{U_{\boldsymbol{m}}(\varphi)||C_{\boldsymbol{z}}(\frac{\pi}{3})\}$ and $\{U_{\boldsymbol{n}}(\theta)||C_{\boldsymbol{x}}(\pi)\}$ that leaves the Hamiltonian invariant should satisfy:

$$\{U_{\boldsymbol{m}}(\varphi)\widehat{||C_{\boldsymbol{z}}}(\tfrac{\pi}{3})\}\,|i, \boldsymbol{z}_i \cdot \boldsymbol{\sigma} = \alpha\rangle = e^{i\eta_{i,i+1,\alpha}}|i+1,\ \boldsymbol{z}_{i+1} \cdot \boldsymbol{\sigma} = \alpha\rangle, \quad \text{(S39)}$$

$$\{U_{\boldsymbol{n}}(\theta)\widehat{||C_{\boldsymbol{x}}}(\pi)\}\ \ |i,\ \boldsymbol{z}_i \cdot \boldsymbol{\sigma} = \alpha\rangle = e^{i\rho_{i,7-i,\alpha}}|7-i,\ \boldsymbol{z}_{7-i} \cdot \boldsymbol{\sigma} = \alpha\rangle, \quad \text{(S40)}$$

where $e^{i\eta_{i,i+1,\alpha}}$ and $e^{i\rho_{i,7-i,\alpha}}$ are the possible phase factors induced by spin rotation $U_{\boldsymbol{m}}(\varphi)$ and $U_{\boldsymbol{n}}(\theta)$.

We first consider $\{U_{\boldsymbol{m}}(\varphi)||C_{\boldsymbol{z}}(\frac{\pi}{3})\}$ that possibly emerge in this model. Assumes $\{U_{\boldsymbol{m}}(\varphi)\widehat{||C_{\boldsymbol{z}}}(\frac{\pi}{3})\}$ is the symmetry of the Hamiltonian, we have:

$$\begin{aligned} &\langle i, \boldsymbol{z}_i \cdot \boldsymbol{\sigma} = \alpha|\widehat{H}|j, \boldsymbol{z}_j \cdot \boldsymbol{\sigma} = \beta\rangle \\ &= e^{i(\eta_{j,j+1,\alpha} - \eta_{i,i+1,\alpha})}\langle i+1, \boldsymbol{z}_{i+1} \cdot \boldsymbol{\sigma} = \alpha|\widehat{H}|j+1, \boldsymbol{z}_{j+1} \cdot \boldsymbol{\sigma} = \beta\rangle. \end{aligned} \quad \text{(S41)}$$

If $\eta_{i,\,i+1,\alpha}=0$, we should have $X\left(\phi_i-\phi_j\right)_{\alpha\beta}=X\left(\phi_{i+1}-\phi_{j+1}\right)_{\alpha\beta}$, which implies that $\phi_{i+1}-\phi_i=\phi_{i+2}-\phi_{i+1}\ mod\ 4\pi$. Thus, we should have the relative angles between two neighbor magnetic moments being the same. Then, we can define $\delta_\phi\equiv\phi_{i+1}-\phi_i$. Furthermore, because of the periodicity of this structure, we have $6\delta_\phi=2p\pi,(p=0,1,\ldots,5)$. So we should have

$$\delta_\phi=\frac{2p\pi}{6},(p=0,1,\ldots,5), \tag{S42}$$

so that the Hamiltonian has the symmetry $\{U_{\boldsymbol{m}}(\varphi)||C_{\boldsymbol{z}}(\frac{\pi}{3})\}$ with $\{U_{\boldsymbol{m}}(\varphi)\widehat{||}C_{\boldsymbol{z}}(\frac{\pi}{3})\}\,|i,\boldsymbol{z}_i\cdot\boldsymbol{\sigma}=\alpha\rangle=|i+1,\,\boldsymbol{z}_{i+1}\cdot\boldsymbol{\sigma}=\alpha\rangle$. The $U_{\boldsymbol{m}}(\varphi)$ is spin rotation along the $\boldsymbol{z}$-axis, with $\varphi=\delta_\phi$ and $\boldsymbol{m}=\boldsymbol{z}$. By proper selection of $\rho_{i,\,7-i,\alpha}$, we can show that the Hamiltonian satisfying $\delta_\phi=\frac{2p\pi}{6},(p=0,1,\ldots,5)$ also have $\{U_{\boldsymbol{n}}(\theta)||C_{\boldsymbol{x}}(\pi)\}$ symmetry.

For $\eta_{i,\,i+1,\alpha}\neq0$, simple calculation shows that the Hamiltonian is invariant under $\{U_{\boldsymbol{m}}(\varphi)||C_{\boldsymbol{z}}(\frac{\pi}{3})\}$ if and only if $e^{-i(\eta_{i+1,i+2,1}-\eta_{i,i+1,-1})}=\pm1$. Then, we can see that in addition to the cases appearing when $\eta_{i,\,i+1,\alpha}=0$, we have another case:

$$\phi_{i+1}-\phi_i=-(\phi_{i+2}-\phi_{i+1}), \tag{S43}$$

so that the Hamiltonian is invariant under $\{U_{\boldsymbol{m}}(\varphi)||C_{\boldsymbol{z}}(\frac{\pi}{3})\}$ and $\{U_{\boldsymbol{n}}(\theta)||C_{\boldsymbol{x}}(\pi)\}$ symmetry, shown in Fig. 2(g). We can also see that the symmetry $\{U_{\boldsymbol{m}}(\varphi)||C_{\boldsymbol{z}}(\frac{\pi}{3})\}$ of the Hamiltonian have $\boldsymbol{m}=cos(\frac{\phi_{i+1}+\phi_i}{2})\hat{\boldsymbol{x}}+sin(\frac{\phi_{i+1}+\phi_i}{2})\hat{\boldsymbol{y}}$, and $\varphi=\pi=\frac{2*3*\pi}{6}$.

In conclusion, symmetry of single-electron Hamiltonian of the form $\{U_{\boldsymbol{m}}(\varphi)||C_{\boldsymbol{n}}\left(\frac{2\pi}{d}\right)\}$ should have the spin rotation angle φ being integer multiple of spatial rotation angle $\frac{2\pi}{d}$:

$$\varphi=\frac{2p\pi}{d},(p=0,1,\ldots,d-1). \tag{S44}$$

The seven different spin arrangements that have spin group symmetry $\{U_{\boldsymbol{m}}(\varphi)||C_{\boldsymbol{z}}(\frac{\pi}{3})\}$ and $\{U_{\boldsymbol{n}}(\theta)||C_{\boldsymbol{x}}(\pi)\}$ are shown in Fig. S1(b-h). These cases show that the axes of spin and spatial rotations can be different, and the rotation angle of spin and spatial rotation can be different, making it necessary for us to implement spin group symmetry. Because a type of spin group includes spin groups with the relative angle between spin rotation axes and spatial rotation axes to be any value, these 7 cases correspond to 4 different types of nontrivial SPG, ${}^{1}6^{1}2^{1}2$, ${}^{6_z}6^{2_x}2^{2_l}2$, ${}^{3_z}6^{2_x}2^{2_{xy}}2$ and ${}^{2}6^{1}2^{2}2$. If considering the full SPG, we will get five types, ${}^{1}6^{1}2^{1}2^{\infty m}1$, ${}^{\bar{1}}6^{1}2^{\bar{1}}2^{\infty m}1$, ${}^{6_z}6^{2_x}2^{2_l}2^{m_z}1$, ${}^{3_z}6^{2_x}2^{2_{xy}}2^{m_z}1$, and ${}^{2}6^{1}2^{2}2^{m_z}1$ with the corresponding magnetic structures written as CL-FM, CL-AFM, NCL1-AFM, NCL2-AFM, and NCL3-FM, as shown in Fig. S1(b-h).

On the other hand, when considering the MPG of the five types of magnetic structures, the symmetry group will not have $C_{\boldsymbol{z}}(\frac{\pi}{3})$ symmetry in general. In addition, the MPG will undoubtedly change under the rotation of all magnetic moments by the same angle, while SPG will not. The hierarchy from SPGs to MPGs for various spin arrangements is shown in Fig. S1(i).

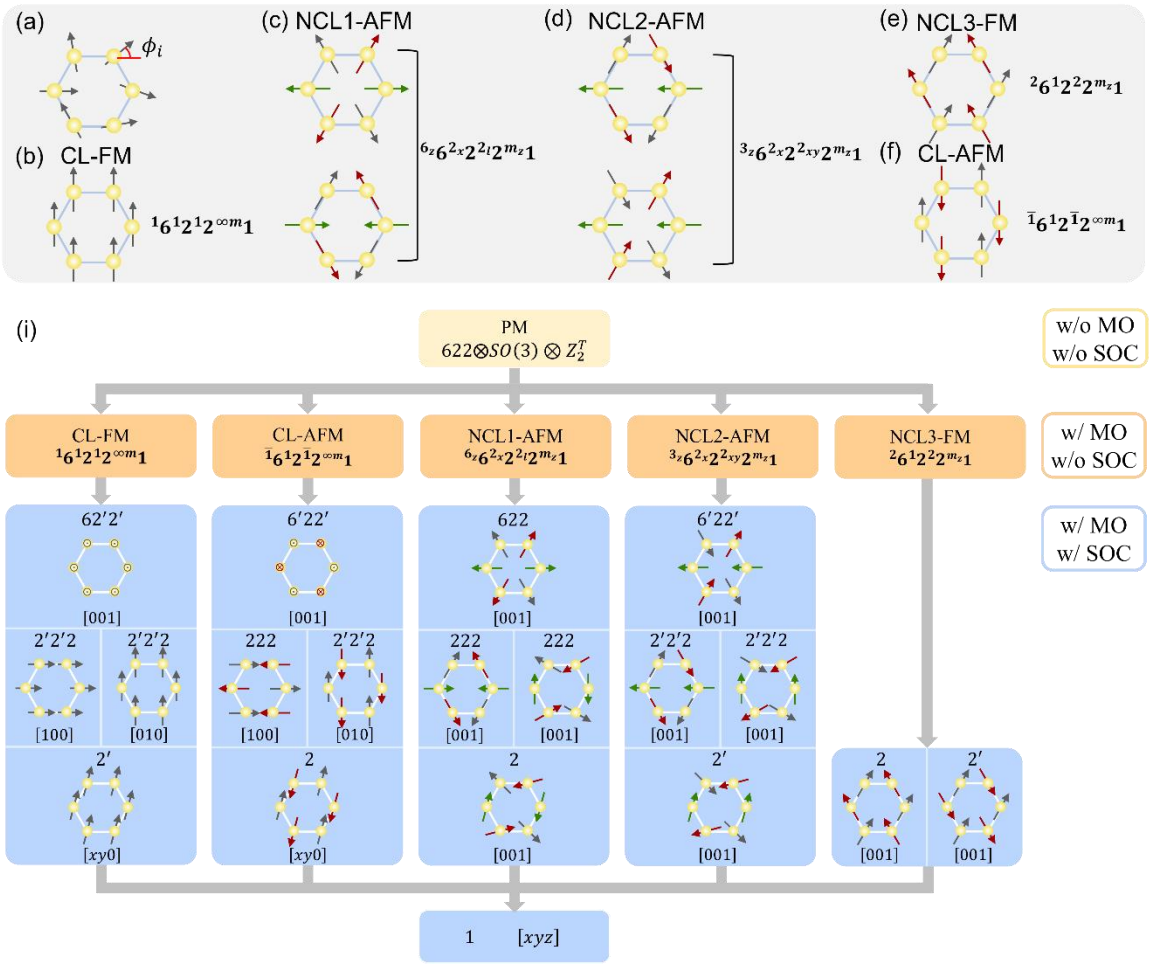

FIG. S1. Symmetries of various spin configurations within the regime of spin point group. (a) a spinful hexagonal molecule with six sites and random in-plane local magnetic moments. (b-h), 7 spin arrangements of the hexagonal and the corresponding five full SPG. (i) symmetry hierarchy from SPGs to MPGs for various spin arrangements. For collinear arrangements, [xyz] denotes the direction of the moments; for noncollinear arrangements, [xyz] denotes the spin rotational axis. CL: colinear; NCL: noncollinear; PM: paramagnetic. For consistency, we use Hermann–Mauguin notation here.

IV. LIST OF THE SPGS FOR COPLANAR AND COLLINEAR SPIN ARRANGEMENTS

In these tables, we follow the modified international notation for spin point group in Ref. [38], which writes spin operations as pre-superscripts of spatial operations. For example, a spin group denoted as ${}^{2}4/{}^{2}m$ represents the spin group with the spatial part being $4/m$ (C_{4h}), and the spin part being 2 (C_2). The 4-fold spatial rotation in this group is combined with 2-fold spin rotation, and the spatial mirror is combined with the same 2-fold spin rotation. For the spin groups with multiple rotation axes, subindices are used in the notations of spin rotation. For instance, the group ${}^{2_z}4/{}^{2_x}m$ represents a spin group with the spatial part being $4/m$ and the spin part being 222 (D_2). The 4-fold spatial rotation in this group is combined with a $U_{\boldsymbol{z}}(\pi)$ spin rotation while the spatial mirror is combined with a $U_{\boldsymbol{x}}(\pi)$ spin rotation.

For the coplanar types of spin point group, ${}^{m}1$ implies the existence of a spin mirror symmetry combined with no spatial operation, i.e., $\{TU_{\boldsymbol{n}}(\pi)||E\}$ (recall that T acts as "inversion" in spin space). For the collinear spin groups, ${}^{\infty m}1$ means the existence of the subgroup $SO(2) \rtimes Z_2^K$ or $C_{\infty v}$ in this group. For the collinear types of spin point group, we note that $SO(2) \rtimes Z_2^K$ is actually the $C_{\infty v}$ group, in Schoenflies notation, acting on spin space. Hermann–Mauguin notation is used in the tables, which writes $C_{\infty v}$ as ∞m.

TABLE S1. Category-I SPGs of the form $G_{NSP} \times Z_2^K$, i.e., the types the spin part of which could be chosen as $G_{\mathrm{NSP}}^{s} = C_1$ is shown in this table. There are 32 types in total.

G_{p0}	N_{p0}	G_{NSP}	$G_{\mathrm{SP}} = G_{\mathrm{NSP}} \times Z_2^K$
1	1	${}^{1}1$	${}^{m}1$
$\bar{1}$	$\bar{1}$	${}^{1}\bar{1}$	${}^{1}\bar{1}{}^{m}1$

2	2	${}^{1}2$	${}^{1}2^{m}1$
m	m	${}^{1}m$	${}^{1}m^{m}1$
$2/m$	$2/m$	${}^{1}2/{}^{1}m$	${}^{1}2/{}^{1}m^{m}1$
$mm2$	$mm2$	${}^{1}m{}^{1}m{}^{1}2$	${}^{1}m{}^{1}m{}^{1}2^{m}1$
222	222	${}^{1}2{}^{1}2{}^{1}2$	${}^{1}2{}^{1}2{}^{1}2^{m}1$
mmm	mmm	${}^{1}m{}^{1}m{}^{1}m$	${}^{1}m{}^{1}m{}^{1}m^{m}1$
4	4	${}^{1}4$	${}^{1}4^{m}1$
$\bar{4}$	$\bar{4}$	${}^{1}\bar{4}$	${}^{1}\bar{4}^{m}1$
$4/m$	$4/m$	${}^{1}4/{}^{1}m$	${}^{1}4/{}^{1}m^{m}1$
422	422	${}^{1}4{}^{1}2{}^{1}2$	${}^{1}4{}^{1}2{}^{1}2^{m}1$
$4mm$	$4mm$	${}^{1}4{}^{1}m{}^{1}m$	${}^{1}4{}^{1}m{}^{1}m^{m}1$
$\bar{4}2m$	$\bar{4}2m$	${}^{1}\bar{4}{}^{1}2{}^{1}m$	${}^{1}\bar{4}{}^{1}2{}^{1}m^{m}1$
$4/mmm$	$4/mmm$	${}^{1}4/{}^{1}m{}^{1}m{}^{1}m$	${}^{1}4/{}^{1}m{}^{1}m{}^{1}m^{m}1$
3	3	${}^{1}3$	${}^{1}3^{m}1$
$\bar{3}$	$\bar{3}$	${}^{1}\bar{3}$	${}^{1}\bar{3}^{m}1$
32	32	${}^{1}3{}^{1}2$	${}^{1}3{}^{1}2^{m}1$
$3m$	$3m$	${}^{1}3{}^{1}m$	${}^{1}3{}^{1}m^{m}1$
$\bar{3}m$	$\bar{3}m$	${}^{1}\bar{3}{}^{1}m$	${}^{1}\bar{3}{}^{1}m^{m}1$
$\bar{6}$	$\bar{6}$	${}^{1}\bar{6}$	${}^{1}\bar{6}^{m}1$
6	6	${}^{1}6$	${}^{1}6^{m}1$
622	622	${}^{1}6{}^{1}2{}^{1}2$	${}^{1}6{}^{1}2{}^{1}2^{m}1$
$6/m$	$6/m$	${}^{1}6/{}^{1}m$	${}^{1}6/{}^{1}m^{m}1$
$6mm$	$6mm$	${}^{1}6{}^{1}m{}^{1}m$	${}^{1}6{}^{1}m{}^{1}m^{m}1$
$\bar{6}m2$	$\bar{6}m2$	${}^{1}\bar{6}{}^{1}m{}^{1}2$	${}^{1}\bar{6}{}^{1}m{}^{1}2^{m}1$
$6/mmm$	$6/mmm$	${}^{1}6/{}^{1}m{}^{1}m{}^{1}m$	${}^{1}6/{}^{1}m{}^{1}m{}^{1}m^{m}1$
23	23	${}^{1}2{}^{1}3$	${}^{1}2{}^{1}3^{m}1$
$2/m\bar{3}$	$2/m\bar{3}$	${}^{1}2/{}^{1}m{}^{1}\bar{3}$	${}^{1}2/{}^{1}m{}^{1}\bar{3}^{m}1$
$\bar{4}3m$	$\bar{4}3m$	${}^{1}\bar{4}{}^{1}3{}^{1}m$	${}^{1}\bar{4}{}^{1}3{}^{1}m^{m}1$
432	432	${}^{1}4{}^{1}3{}^{1}2$	${}^{1}4{}^{1}3{}^{1}2^{m}1$
$4/m\bar{3}2/m$	$4/m\bar{3}2/m$	${}^{1}4/{}^{1}m{}^{1}\bar{3}{}^{1}2/{}^{1}m$	${}^{1}4/{}^{1}m{}^{1}\bar{3}{}^{1}2/{}^{1}m^{m}1$

TABLE S2. Category-II SPGs of the form $G_{NSP} \times Z_2^K$, i.e., the types the spin part of which could be chosen as $G_{\mathrm{NSP}}^{s} = C_2$ and the direction $\boldsymbol{n}$ of which is parallel to the $\boldsymbol{z}$-axis is shown in this table. There are 58 types in total.

G_{p0}	N_{p0}	G_{NSP}	$G_{\mathrm{SP}} = G_{\mathrm{NSP}} \times Z_2^K$
$\bar{1}$	1	${}^{2}\bar{1}$	${}^{2_z}\bar{1}^{m_z}1$

2	1	$^{2}2$	$^{2_z}2^{m_z}1$
m	1	^{2}m	$^{2_z}m^{m_z}1$
$2/m$	2	$^{1}2/^{2}m$	$^{2_z}2/^{2}m^{m_z}1$
$2/m$	m	$^{2}2/^{1}m$	$^{2_z}2/^{1}m^{m_z}1$
$2/m$	$\bar{1}$	$^{2}2/^{2}m$	$^{2_z}2/^{2}m^{m_z}1$
$mm2$	2	$^{2}m^{2}m^{1}2$	$^{2_z}m^{2_z}m^{1}2^{m_z}1$
$mm2$	m	$^{1}m^{2}m^{2}2$	$^{1}m^{2_z}m^{2_z}2^{m_z}1$
222	2	$^{1}2^{2}2^{2}2$	$^{1}2^{2_z}2^{2_z}2^{m_z}1$
mmm	$2/m$	$^{1}m^{2}m^{2}m$	$^{1}m^{2_z}m^{2_z}m^{m_z}1$
mmm	$mm2$	$^{1}m^{1}m^{2}m$	$^{1}m^{1}m^{2_z}m^{m_z}1$
mmm	222	$^{2}m^{2}m^{2}m$	$^{2_z}m^{2_z}m^{2_z}m^{m_z}1$
4	2	$^{2}4$	$^{2_z}4^{m_z}1$
$\bar{4}$	2	$^{2}\bar{4}$	$^{2_z}\bar{4}^{m_z}1$
$4/m$	$2/m$	$^{2}4/^{1}m$	$^{2_z}4/^{1}m^{m_z}1$
$4/m$	$\bar{4}$	$^{2}4/^{2}m$	$^{2_z}4/^{2_z}m^{m_z}1$
$4/m$	4	$^{1}4/^{2}m$	$^{1}4/^{2_z}m^{m_z}1$
422	4	$^{1}4^{2}2^{2}2$	$^{1}4^{2_z}2^{2_z}2^{m_z}1$
422	222	$^{2}4^{1}2^{2}2$	$^{2_z}4^{1}2^{2_z}2^{m_z}1$
$4mm$	4	$^{1}4^{2}m^{2}m$	$^{1}4^{2_z}m^{2_z}m^{m_z}1$
$4mm$	$mm2$	$^{2}4^{1}m^{2}m$	$^{2_z}4^{1}m^{2_z}m^{m_z}1$
$\bar{4}2m$	$\bar{4}$	$^{1}\bar{4}^{2}2^{2}m$	$^{1}\bar{4}^{2_z}2^{2_z}m^{m_z}1$
$\bar{4}2m$	$mm2$	$^{2}\bar{4}^{2}2^{1}m$	$^{2_z}\bar{4}^{2_z}2^{1}m^{m_z}1$
$\bar{4}2m$	222	$^{2}\bar{4}^{1}2^{2}m$	$^{2_z}\bar{4}^{1}2^{2_z}m^{m_z}1$
$4/mmm$	$\bar{4}2m$	$^{2}4/^{2}m^{2}m^{1}m$	$^{2}4/^{2_z}m^{2_z}m^{1}m^{m_z}1$
$4/mmm$	$4mm$	$^{1}4/^{2}m^{1}m^{1}m$	$^{1}4/^{2_z}m^{1}m^{1}m^{m_z}1$
$4/mmm$	mmm	$^{2}4/^{1}m^{1}m^{2}m$	$^{2_z}4/^{1}m^{1}m^{2_z}m^{m_z}1$
$4/mmm$	$4/m$	$^{1}4/^{1}m^{2}m^{2}m$	$^{1}4/^{1}m^{2_z}m^{2_z}m^{m_z}1$
$4/mmm$	422	$^{1}4/^{2}m^{2}m^{2}m$	$^{1}4/^{2_z}m^{2_z}m^{2_z}m^{m_z}1$
$\bar{3}$	3	$^{2}\bar{3}$	$^{2_z}\bar{3}^{m_z}1$
32	3	$^{1}3^{2}2$	$^{1}3^{2_z}2^{m_z}1$
$3m$	3	$^{1}3^{2}m$	$^{1}3^{2_z}m^{m_z}1$
$\bar{3}m$	$\bar{3}$	$^{1}\bar{3}^{2}m$	$^{1}\bar{3}^{2_z}m^{m_z}1$
$\bar{3}m$	$3m$	$^{2}\bar{3}^{1}m$	$^{2_z}\bar{3}^{1}m^{m_z}1$
$\bar{3}m$	32	$^{2}\bar{3}^{2}m$	$^{2_z}\bar{3}^{2_z}m^{m_z}1$
$\bar{6}$	3	$^{2}\bar{6}$	$^{2_z}\bar{6}^{m_z}1$
6	3	$^{2}6$	$^{2_z}6^{m_z}1$
622	6	$^{1}6^{2}2^{2}2$	$^{1}6^{2_z}2^{2_z}2^{m_z}1$

622	32	${}^{2}6{}^{1}2{}^{2}2$	${}^{2_z}6{}^{1}2{}^{2_z}2{}^{m_z}1$
$6/m$	$\bar{3}$	${}^{2}6/{}^{2}m$	${}^{2_z}6/{}^{2_z}m{}^{m_z}1$
$6/m$	$\bar{6}$	${}^{2}6/{}^{1}m$	${}^{2_z}6/{}^{1}m{}^{m_z}1$
$6/m$	6	${}^{1}6/{}^{2}m$	${}^{1}6/{}^{2_z}m{}^{m_z}1$
$6mm$	6	${}^{1}6{}^{2}m{}^{2}m$	${}^{1}6{}^{2_z}m{}^{2_z}m{}^{m_z}1$
$6mm$	$3m$	${}^{2}6{}^{1}m{}^{2}m$	${}^{2_z}6{}^{1}m{}^{2_z}m{}^{m_z}1$
$\bar{6}m2$	$\bar{6}$	${}^{1}\bar{6}{}^{2}m{}^{2}2$	${}^{1}\bar{6}{}^{2_z}m{}^{2_z}2{}^{m_z}1$
$\bar{6}m2$	$3m$	${}^{2}\bar{6}{}^{1}m{}^{2}2$	${}^{2_z}\bar{6}{}^{1}m{}^{2_z}2{}^{m_z}1$
$\bar{6}m2$	32	${}^{2}\bar{6}{}^{2}m{}^{1}2$	${}^{2_z}\bar{6}{}^{2_z}m{}^{1}2{}^{m_z}1$
$6/mmm$	$\bar{3}m$	${}^{2}6/{}^{2}m{}^{1}m{}^{2}m$	${}^{2_z}6/{}^{2_z}m{}^{1}m{}^{2_z}m{}^{m_z}1$
$6/mmm$	$\bar{6}m2$	${}^{2}6/{}^{1}m{}^{2}m{}^{1}m$	${}^{2_z}6/{}^{1}m{}^{2_z}m{}^{1}m{}^{m_z}1$
$6/mmm$	$6/m$	${}^{1}6/{}^{1}m{}^{2}m{}^{2}m$	${}^{1}6/{}^{1}m{}^{2_z}m{}^{2_z}m{}^{m_z}1$
$6/mmm$	$6mm$	${}^{1}6/{}^{2}m{}^{1}m{}^{1}m$	${}^{1}6/{}^{2_z}m{}^{1}m{}^{1}m{}^{m_z}1$
$6/mmm$	622	${}^{1}6/{}^{2}m{}^{2}m{}^{2}m$	${}^{1}6/{}^{2_z}m{}^{2_z}m{}^{2_z}m{}^{m_z}1$
$2/m\bar{3}$	23	${}^{1}2/{}^{2}m{}^{2}\bar{3}$	${}^{1}2/{}^{2_z}m{}^{2_z}\bar{3}{}^{m_z}1$
$\bar{4}3m$	23	${}^{2}\bar{4}{}^{1}3{}^{2}m$	${}^{2_z}\bar{4}{}^{1}3{}^{2_z}m{}^{m_z}1$
432	23	${}^{2}4{}^{1}3{}^{2}2$	${}^{2_z}4{}^{1}3{}^{2_z}2{}^{m_z}1$
$4/m\bar{3}2/m$	$2/m\bar{3}$	${}^{2}4/{}^{1}m{}^{1}\bar{3}{}^{2}2/{}^{2}m$	${}^{2_z}4/{}^{1}m{}^{1}\bar{3}{}^{2_z}2/{}^{2_z}m{}^{m_z}1$
$4/m\bar{3}2/m$	$\bar{4}3m$	${}^{2}4/{}^{2}m{}^{2}\bar{3}{}^{2}2/{}^{1}m$	${}^{2_z}4/{}^{2_z}m{}^{2_z}\bar{3}{}^{2_z}2/{}^{1}m{}^{m_z}1$
$4/m\bar{3}2/m$	432	${}^{1}4/{}^{2}m{}^{2}\bar{3}{}^{1}2/{}^{2}m$	${}^{1}4/{}^{2_z}m{}^{2_z}\bar{3}{}^{1}2/{}^{2_z}m{}^{m_z}1$

TABLE S3. Category-III SPGs of the form $G_{NSP} \times Z_2^K$, i.e., the types the spin part of which could be chosen as $G_{\mathrm{NSP}}^{s} = C_2$ and the direction $\boldsymbol{n}$ of which is parallel to the $\boldsymbol{x}$-axis is shown in this table. There are 58 types in total.

G_{p0}	N_{p0}	G_{NSP}	$G_{\mathrm{SP}} = G_{\mathrm{NSP}} \times Z_2^K$
$\bar{1}$	1	${}^{2}\bar{1}$	${}^{2_z}\bar{1}{}^{m_x}1$
2	1	${}^{2}2$	${}^{2_z}2{}^{m_x}1$
m	1	${}^{2}m$	${}^{2_z}m{}^{m_x}1$
$2/m$	2	${}^{1}2/{}^{2}m$	${}^{2_z}2/{}^{2}m{}^{m_x}1$
$2/m$	m	${}^{2}2/{}^{1}m$	${}^{2_z}2/{}^{1}m{}^{m_x}1$
$2/m$	$\bar{1}$	${}^{2}2/{}^{2}m$	${}^{2_z}2/{}^{2}m{}^{m_x}1$
$mm2$	2	${}^{2}m{}^{2}m{}^{1}2$	${}^{2_z}m{}^{2_z}m{}^{1}2{}^{m_x}1$
$mm2$	m	${}^{1}m{}^{2}m{}^{2}2$	${}^{1}m{}^{2_z}m{}^{2_z}2{}^{m_x}1$
222	2	${}^{1}2{}^{2}2{}^{2}2$	${}^{1}2{}^{2_z}2{}^{2_z}2{}^{m_x}1$
mmm	$2/m$	${}^{1}m{}^{2}m{}^{2}m$	${}^{1}m{}^{2_z}m{}^{2_z}m{}^{m_x}1$
mmm	$mm2$	${}^{1}m{}^{1}m{}^{2}m$	${}^{1}m{}^{1}m{}^{2_z}m{}^{m_x}1$

mmm	222	${}^{2}m{}^{2}m{}^{2}m$	${}^{2_z}m{}^{2_z}m{}^{2_z}m{}^{m_x}1$
4	2	${}^{2}4$	${}^{2_z}4{}^{m_x}1$
$\bar{4}$	2	${}^{2}\bar{4}$	${}^{2_z}\bar{4}{}^{m_x}1$
$4/m$	$2/m$	${}^{2}4/{}^{1}m$	${}^{2_z}4/{}^{1}m{}^{m_x}1$
$4/m$	$\bar{4}$	${}^{2}4/{}^{2}m$	${}^{2_z}4/{}^{2_z}m{}^{m_x}1$
$4/m$	4	${}^{1}4/{}^{2}m$	${}^{1}4/{}^{2_z}m{}^{m_x}1$
422	4	${}^{1}4{}^{2}2{}^{2}2$	${}^{1}4{}^{2_z}2{}^{2_z}2{}^{m_x}1$
422	222	${}^{2}4{}^{1}2{}^{2}2$	${}^{2_z}4{}^{1}2{}^{2_z}2{}^{m_x}1$
$4mm$	4	${}^{1}4{}^{2}m{}^{2}m$	${}^{1}4{}^{2_z}m{}^{2_z}m{}^{m_x}1$
$4mm$	$mm2$	${}^{2}4{}^{1}m{}^{2}m$	${}^{2_z}4{}^{1}m{}^{2_z}m{}^{m_x}1$
$\bar{4}2m$	$\bar{4}$	${}^{1}\bar{4}{}^{2}2{}^{2}m$	${}^{1}\bar{4}{}^{2_z}2{}^{2_z}m{}^{m_x}1$
$\bar{4}2m$	$mm2$	${}^{2}\bar{4}{}^{2}2{}^{1}m$	${}^{2_z}\bar{4}{}^{2_z}2{}^{1}m{}^{m_x}1$
$\bar{4}2m$	222	${}^{2}\bar{4}{}^{1}2{}^{2}m$	${}^{2_z}\bar{4}{}^{1}2{}^{2_z}m{}^{m_x}1$
$4/mmm$	$\bar{4}2m$	${}^{2}4/{}^{2}m{}^{2}m{}^{1}m$	${}^{2}4/{}^{2_z}m{}^{2_z}m{}^{1}m{}^{m_x}1$
$4/mmm$	$4mm$	${}^{1}4/{}^{2}m{}^{1}m{}^{1}m$	${}^{1}4/{}^{2_z}m{}^{1}m{}^{1}m{}^{m_x}1$
$4/mmm$	mmm	${}^{2}4/{}^{1}m{}^{1}m{}^{2}m$	${}^{2_z}4/{}^{1}m{}^{1}m{}^{2_z}m{}^{m_x}1$
$4/mmm$	$4/m$	${}^{1}4/{}^{1}m{}^{2}m{}^{2}m$	${}^{1}4/{}^{1}m{}^{2_z}m{}^{2_z}m{}^{m_x}1$
$4/mmm$	422	${}^{1}4/{}^{2}m{}^{2}m{}^{2}m$	${}^{1}4/{}^{2_z}m{}^{2_z}m{}^{2_z}m{}^{m_x}1$
$\bar{3}$	3	${}^{2}\bar{3}$	${}^{2_z}\bar{3}{}^{m_x}1$
32	3	${}^{1}3{}^{2}2$	${}^{1}3{}^{2_z}2{}^{m_x}1$
$3m$	3	${}^{1}3{}^{2}m$	${}^{1}3{}^{2_z}m{}^{m_x}1$
$\bar{3}m$	$\bar{3}$	${}^{1}\bar{3}{}^{2}m$	${}^{1}\bar{3}{}^{2_z}m{}^{m_x}1$
$\bar{3}m$	$3m$	${}^{2}\bar{3}{}^{1}m$	${}^{2_z}\bar{3}{}^{1}m{}^{m_x}1$
$\bar{3}m$	32	${}^{2}\bar{3}{}^{2}m$	${}^{2_z}\bar{3}{}^{2_z}m{}^{m_x}1$
$\bar{6}$	3	${}^{2}\bar{6}$	${}^{2_z}\bar{6}{}^{m_x}1$
6	3	${}^{2}6$	${}^{2_z}6{}^{m_x}1$
622	6	${}^{1}6{}^{2}2{}^{2}2$	${}^{1}6{}^{2_z}2{}^{2_z}2{}^{m_x}1$
622	32	${}^{2}6{}^{1}2{}^{2}2$	${}^{2_z}6{}^{1}2{}^{2_z}2{}^{m_x}1$
$6/m$	$\bar{3}$	${}^{2}6/{}^{2}m$	${}^{2_z}6/{}^{2_z}m{}^{m_x}1$
$6/m$	$\bar{6}$	${}^{2}6/{}^{1}m$	${}^{2_z}6/{}^{1}m{}^{m_x}1$
$6/m$	6	${}^{1}6/{}^{2}m$	${}^{1}6/{}^{2_z}m{}^{m_x}1$
$6mm$	6	${}^{1}6{}^{2}m{}^{2}m$	${}^{1}6{}^{2_z}m{}^{2_z}m{}^{m_x}1$
$6mm$	$3m$	${}^{2}6{}^{1}m{}^{2}m$	${}^{2_z}6{}^{1}m{}^{2_z}m{}^{m_x}1$
$\bar{6}m2$	$\bar{6}$	${}^{1}\bar{6}{}^{2}m{}^{2}2$	${}^{1}\bar{6}{}^{2_z}m{}^{2_z}2{}^{m_x}1$
$\bar{6}m2$	$3m$	${}^{2}\bar{6}{}^{1}m{}^{2}2$	${}^{2_z}\bar{6}{}^{1}m{}^{2_z}2{}^{m_x}1$
$\bar{6}m2$	32	${}^{2}\bar{6}{}^{2}m{}^{1}2$	${}^{2_z}\bar{6}{}^{2_z}m{}^{1}2{}^{m_x}1$
$6/mmm$	$\bar{3}m$	${}^{2}6/{}^{2}m{}^{1}m{}^{2}m$	${}^{2_z}6/{}^{2_z}m{}^{1}m{}^{2_z}m{}^{m_x}1$

$6/mmm$	$\bar{6}m2$	${}^{2}6/{}^{1}m{}^{2}m{}^{1}m$	${}^{2_z}6/{}^{1}m{}^{2_z}m{}^{1}m{}^{m_x}1$
$6/mmm$	$6/m$	${}^{1}6/{}^{1}m{}^{2}m{}^{2}m$	${}^{1}6/{}^{1}m{}^{2_z}m{}^{2_z}m{}^{m_x}1$
$6/mmm$	$6mm$	${}^{1}6/{}^{2}m{}^{1}m{}^{1}m$	${}^{1}6/{}^{2_z}m{}^{1}m{}^{1}m{}^{m_x}1$
$6/mmm$	622	${}^{1}6/{}^{2}m{}^{2}m{}^{2}m$	${}^{1}6/{}^{2_z}m{}^{2_z}m{}^{2_z}m{}^{m_x}1$
$2/m\bar{3}$	23	${}^{1}2/{}^{2}m{}^{2}\bar{3}$	${}^{1}2/{}^{2_z}m{}^{2_z}\bar{3}{}^{m_x}1$
$\bar{4}3m$	23	${}^{2}\bar{4}{}^{1}3{}^{2}m$	${}^{2_z}\bar{4}{}^{1}3{}^{2_z}m{}^{m_x}1$
432	23	${}^{2}4{}^{1}3{}^{2}2$	${}^{2_z}4{}^{1}3{}^{2_z}2{}^{m_x}1$
$4/m\bar{3}2/m$	$2/m\bar{3}$	${}^{2}4/{}^{1}m{}^{1}\bar{3}{}^{2}2/{}^{2}m$	${}^{2_z}4/{}^{1}m{}^{1}\bar{3}{}^{2_z}2/{}^{2_z}m{}^{m_x}1$
$4/m\bar{3}2/m$	$\bar{4}3m$	${}^{2}4/{}^{2}m{}^{2}\bar{3}{}^{2}2/{}^{1}m$	${}^{2_z}4/{}^{2_z}m{}^{2_z}\bar{3}{}^{2_z}2/{}^{1}m{}^{m_x}1$
$4/m\bar{3}2/m$	432	${}^{1}4/{}^{2}m{}^{2}\bar{3}{}^{1}2/{}^{2}m$	${}^{1}4/{}^{2_z}m{}^{2_z}\bar{3}{}^{1}2/{}^{2_z}m{}^{m_x}1$

TABLE S4. Category-IV SPGs of the form $G_{NSP} \times Z_2^K$, i.e., the types the spin part of which could be chosen as $G_{\mathrm{NSP}}^{s} = C_3$ and the direction $\boldsymbol{n}$ of which is parallel to the $\boldsymbol{z}$-axis is shown in this table. There are 7 types in total.

G_{p0}	N_{p0}	G_{NSP}	$G_{\mathrm{SP}} = G_{\mathrm{NSP}} \times Z_2^K$
3	1	${}^{3}3$	${}^{3_z}3{}^{m_z}1$
$\bar{3}$	$\bar{1}$	${}^{3}\bar{3}$	${}^{3_z}\bar{3}{}^{m_z}1$
$\bar{6}$	m	${}^{3}\bar{6}$	${}^{3_z}\bar{6}{}^{m_z}1$
6	2	${}^{3}6$	${}^{3_z}6{}^{m_z}1$
$6/m$	$2/m$	${}^{3}6/{}^{1}m$	${}^{3_z}6/{}^{1}m{}^{m_z}1$
23	222	${}^{1}2{}^{3}3$	${}^{1}2{}^{3_z}3{}^{m_z}1$
$m\bar{3}$	mmm	${}^{1}m{}^{3}\bar{3}$	${}^{1}m{}^{3_z}\bar{3}{}^{m_z}1$

TABLE S5. Category-V SPGs of the form $G_{NSP} \times Z_2^K$, i.e., the types the spin part of which could be chosen as $G_{\mathrm{NSP}}^{s} = C_4$ and the direction $\boldsymbol{n}$ of which is parallel to the $\boldsymbol{z}$-axis is shown in this table. There are 4 types in total.

G_{p0}	N_{p0}	G_{NSP}	$G_{\mathrm{SP}} = G_{\mathrm{NSP}} \times Z_2^K$
4	1	${}^{4}4$	${}^{4_z}4{}^{m_z}1$
$\bar{4}$	$\bar{1}$	${}^{4}\bar{4}$	${}^{4_z}\bar{4}{}^{m_z}1$
$4/m$	$\bar{1}$	${}^{4}4/{}^{2}m$	${}^{4_z}4/{}^{2_z}m{}^{m_z}1$
$4/m$	m	${}^{4}4/{}^{1}m$	${}^{4_z}4/{}^{1}m{}^{m_z}1$

TABLE S6. Category-VI SPGs of the form $G_{NSP} \times Z_2^K$, i.e., the types the spin part of which could be chosen as $G_{\mathrm{NSP}}^{s} = C_6$ and the direction $\boldsymbol{n}$ of which is parallel to the $\boldsymbol{z}$-axis is shown in this table. There are 7 classes in total.

G_{p0}	N_{p0}	G_{NSP}	$G_{\mathrm{SP}}=G_{\mathrm{NSP}}\times Z_2^K$
$\bar{3}$	1	${}^{6}\bar{3}$	${}^{6_z}\bar{3}^{m_z}1$
$\bar{6}$	1	${}^{6}\bar{6}$	${}^{6_z}\bar{6}^{m_z}1$
6	1	${}^{6}6$	${}^{6_z}6^{m_z}1$
$6/m$	2	${}^{3}6/{}^{2}m$	${}^{3_z}6/{}^{2_z}m^{m_z}1$
$6/m$	m	${}^{6}6/{}^{1}m$	${}^{6_z}6/{}^{1}m^{m_z}1$
$6/m$	$\bar{1}$	${}^{6}6/{}^{2}m$	${}^{6_z}6/{}^{2_z}m^{m_z}1$
$2/m\bar{3}$	222	${}^{1}2/{}^{2}m{}^{6}\bar{3}$	${}^{1}2/{}^{2_z}m{}^{6_z}\bar{3}^{m_z}1$

TABLE S7. Category-VII SPGs of the form $G_{NSP}\times Z_2^K$, i.e., the types the spin part of which could be chosen as $G_{\mathrm{NSP}}^{s}=D_2$ and the direction $\boldsymbol{n}$ of which is parallel to the $\boldsymbol{x}$-, $\boldsymbol{y}$- or $\boldsymbol{z}$-axis when the three directions lead to identical classes, is shown in this table. There are 2 types in total.

G_{p0}	N_{p0}	G_{NSP}	$G_{\mathrm{SP}}=G_{\mathrm{NSP}}\times Z_2^K$
222	1	${}^{2_x}2{}^{2_y}2{}^{2_z}2$	${}^{2_x}2{}^{2_y}2{}^{2_z}2^{m_z}1$
mmm	$\bar{1}$	${}^{2_x}m{}^{2_y}m{}^{2_z}m$	${}^{2_x}m{}^{2_y}m{}^{2_z}m^{m_z}1$

TABLE S8. Category-VIII SPGs of the form $G_{NSP}\times Z_2^K$, i.e., the types the spin part of which could be chosen as $G_{\mathrm{NSP}}^{s}=D_2$ and the direction $\boldsymbol{n}$ of which is parallel to the x-, y- or $\boldsymbol{z}$-axis when the three directions lead to different types, is shown in this table. There are 62 types in total.

G_{p0}	N_{p0}	G_{NSP}	$G_{\mathrm{SP}}=G_{\mathrm{NSP}}\times Z_2^K$
$2/m$	1	${}^{2_z}2/{}^{2_x}m$	${}^{2_z}2/{}^{2_x}m^{m_x}1$
			${}^{2_z}2/{}^{2_x}m^{m_y}1$
			${}^{2_z}2/{}^{2_x}m^{m_z}1$
$mm2$	1	${}^{2_x}m{}^{2_y}m{}^{2_z}2$	${}^{2_x}m{}^{2_y}m{}^{2_z}2^{m_x}1$
			${}^{2_x}m{}^{2_y}m{}^{2_z}2^{m_z}1$
mmm	2	${}^{2_z}m{}^{2_z}m{}^{2_x}m$	${}^{2_z}m{}^{2_z}m{}^{2_x}m^{m_x}1$
			${}^{2_z}m{}^{2_z}m{}^{2_x}m^{m_y}1$
			${}^{2_z}m{}^{2_z}m{}^{2_x}m^{m_z}1$
mmm	m	${}^{2_x}m{}^{2_y}m{}^{1}m$	${}^{2_x}m{}^{2_y}m{}^{1}m^{m_x}1$
			${}^{2_x}m{}^{2_y}m{}^{1}m^{m_z}1$
$4/m$	2	${}^{2_z}4/{}^{2_x}m$	${}^{2_z}4/{}^{2_x}m^{m_x}1$
			${}^{2_z}4/{}^{2_x}m^{m_y}1$
			${}^{2_z}4/{}^{2_x}m^{m_z}1$

422	2	${}^{2_x}4^{2_y}2^{2_z}2$	${}^{2_x}4^{2_y}2^{2_z}2^{m_x}1$
			${}^{2_x}4^{2_y}2^{2_z}2^{m_y}1$
$4mm$	2	${}^{2_x}4^{2_y}m^{2_z}m$	${}^{2_x}4^{2_y}m^{2_z}m^{m_x}1$
			${}^{2_x}4^{2_y}m^{2_z}m^{m_y}1$
$\bar{4}2m$	2	${}^{2_x}\bar{4}^{2_y}2^{2_z}m$	${}^{2_x}\bar{4}^{2_y}2^{2_z}m^{m_x}1$
			${}^{2_x}\bar{4}^{2_y}2^{2_z}m^{m_y}1$
			${}^{2_x}\bar{4}^{2_y}2^{2_z}m^{m_z}1$
$4/mmm$	$\bar{4}$	${}^{2_z}4/{}^{2_z}m^{2_x}m^{2_y}m$	${}^{2_z}4/{}^{2_z}m^{2_x}m^{2_y}m^{m_x}1$
			${}^{2_z}4/{}^{2_z}m^{2_x}m^{2_y}m^{m_z}1$
$4/mmm$	4	${}^{1}4/{}^{2_x}m^{2_y}m^{2_y}m$	${}^{1}4/{}^{2_x}m^{2_y}m^{2_y}m^{m_x}1$
			${}^{1}4/{}^{2_x}m^{2_y}m^{2_y}m^{m_y}1$
			${}^{1}4/{}^{2_x}m^{2_y}m^{2_y}m^{m_z}1$
$4/mmm$	$2/m$	${}^{2_z}4/{}^{1}m^{2_x}m^{2_y}m$	${}^{2_z}4/{}^{1}m^{2_x}m^{2_y}m^{m_x}1$
			${}^{2_z}4/{}^{1}m^{2_x}m^{2_y}m^{m_z}1$
$4/mmm$	$mm2$	${}^{2_z}4/{}^{2_x}m^{1}m^{2_z}m$	${}^{2_z}4/{}^{2_x}m^{1}m^{2_z}m^{m_x}1$
			${}^{2_z}4/{}^{2_x}m^{1}m^{2_z}m^{m_y}1$
			${}^{2_z}4/{}^{2_x}m^{1}m^{2_z}m^{m_z}1$
$4/mmm$	222	${}^{2_z}4/{}^{2_x}m^{2_x}m^{2_y}m$	${}^{2_z}4/{}^{2_x}m^{2_x}m^{2_y}m^{m_x}1$
			${}^{2_z}4/{}^{2_x}m^{2_x}m^{2_y}m^{m_y}1$
			${}^{2_z}4/{}^{2_x}m^{2_x}m^{2_y}m^{m_z}1$
$\bar{3}m$	3	${}^{2_x}\bar{3}^{2_z}m$	${}^{2_x}\bar{3}^{2_z}m^{m_x}1$
			${}^{2_x}\bar{3}^{2_z}m^{m_y}1$
			${}^{2_x}\bar{3}^{2_z}m^{m_z}1$
622	3	${}^{2_x}6^{2_y}2^{2_z}2$	${}^{2_x}6^{2_y}2^{2_z}2^{m_x}1$
			${}^{2_x}6^{2_y}2^{2_z}2^{m_y}1$
$6/m$	3	${}^{2_z}6/{}^{2_x}m$	${}^{2_z}6/{}^{2_x}m^{m_x}1$
			${}^{2_z}6/{}^{2_x}m^{m_y}1$
			${}^{2_z}6/{}^{2_x}m^{m_z}1$
$6mm$	3	${}^{2_x}6^{2_y}m^{2_z}m$	${}^{2_x}6^{2_y}m^{2_z}m^{m_x}1$
			${}^{2_x}6^{2_y}m^{2_z}m^{m_y}1$
$\bar{6}m2$	3	${}^{2_z}\bar{6}^{2_x}m^{2_y}2$	${}^{2_z}\bar{6}^{2_x}m^{2_y}2^{m_x}1$
			${}^{2_z}\bar{6}^{2_x}m^{2_y}2^{m_y}1$
			${}^{2_z}\bar{6}^{2_x}m^{2_y}2^{m_z}1$
$6/mmm$	$\bar{3}$	${}^{2_z}6/{}^{2_z}m^{2_x}m^{2_y}m$	${}^{2_z}6/{}^{2_z}m^{2_x}m^{2_y}m^{m_x}1$
			${}^{2_z}6/{}^{2_z}m^{2_x}m^{2_y}m^{m_z}1$
$6/mmm$	$\bar{6}$	${}^{2_z}6/{}^{1}m^{2_x}m^{2_y}m$	${}^{2_z}6/{}^{1}m^{2_x}m^{2_y}m^{m_x}1$
			${}^{2_z}6/{}^{1}m^{2_x}m^{2_y}m^{m_z}1$

$6/mmm$	6	${}^{1}6/{}^{2_z}m{}^{2_x}m{}^{2_x}m$	${}^{1}6/{}^{2_z}m{}^{2_x}m{}^{2_x}m{}^{m_x}1$
			${}^{1}6/{}^{2_z}m{}^{2_x}m{}^{2_x}m{}^{m_y}1$
			${}^{1}6/{}^{2_z}m{}^{2_x}m{}^{2_x}m{}^{m_z}1$
$6/mmm$	$3m$	${}^{2_z}6/{}^{2_x}m{}^{1}m{}^{2_z}m$	${}^{2_z}6/{}^{2_x}m{}^{1}m{}^{2_z}m{}^{m_x}1$
			${}^{2_z}6/{}^{2_x}m{}^{1}m{}^{2_z}m{}^{m_y}1$
			${}^{2_z}6/{}^{2_x}m{}^{1}m{}^{2_z}m{}^{m_z}1$
$6/mmm$	32	${}^{2_z}6/{}^{2_x}m{}^{2_y}m{}^{2_x}m$	${}^{2_z}6/{}^{2_x}m{}^{2_y}m{}^{2_x}m{}^{m_x}1$
			${}^{2_z}6/{}^{2_x}m{}^{2_y}m{}^{2_x}m{}^{m_y}1$
			${}^{2_z}6/{}^{2_x}m{}^{2_y}m{}^{2_x}m{}^{m_z}1$
$4/m\bar{3}2/m$	23	${}^{2_x}4/{}^{2_y}m{}^{2_y}\bar{3}{}^{2_x}2/{}^{2_z}m$	${}^{2_x}4/{}^{2_y}m{}^{2_y}\bar{3}{}^{2_x}2/{}^{2_z}m{}^{m_x}1$
			${}^{2_x}4/{}^{2_y}m{}^{2_y}\bar{3}{}^{2_x}2/{}^{2_z}m{}^{m_y}1$
			${}^{2_x}4/{}^{2_y}m{}^{2_y}\bar{3}{}^{2_x}2/{}^{2_z}m{}^{m_z}1$

TABLE S9. Category-IX SPGs of the form $G_{NSP} \times Z_2^K$, i.e., the types the spin part of which could be chosen as $G_{\mathrm{NSP}}^{s} = D_3$ and the direction $\boldsymbol{n}$ of which is parallel to the $\boldsymbol{z}$-axis is shown in this table. There are 10 types in total.

G_{p0}	N_{p0}	G_{NSP}	$G_{\mathrm{SP}} = G_{\mathrm{NSP}} \times Z_2^K$
32	1	${}^{3_z}3{}^{2_x}2$	${}^{3_z}3{}^{2_x}2{}^{m_z}1$
$3m$	1	${}^{3_z}3{}^{2_x}m$	${}^{3_z}3{}^{2_x}m{}^{m_z}1$
$\bar{3}m$	$\bar{1}$	${}^{3_z}\bar{3}{}^{2_x}m$	${}^{3_z}\bar{3}{}^{2_x}m{}^{m_z}1$
622	2	${}^{3_z}6{}^{2_x}2{}^{2_{xy}}2$	${}^{3_z}6{}^{2_x}2{}^{2_{xy}}2{}^{m_z}1$
$6mm$	2	${}^{3_z}6{}^{2_x}m{}^{2_{xy}}m$	${}^{3_z}6{}^{2_x}m{}^{2_{xy}}m{}^{m_z}1$
$\bar{6}m2$	m	${}^{3_z}\bar{6}{}^{2_x}m{}^{2_{xy}}2$	${}^{3_z}\bar{6}{}^{2_x}m{}^{2_{xy}}2{}^{m_z}1$
$6/mmm$	$2/m$	${}^{3_z}6/{}^{1}m{}^{2_x}m{}^{2_{xy}}m$	${}^{3_z}6/{}^{1}m{}^{2_x}m{}^{2_{xy}}m{}^{m_z}1$
$\bar{4}3m$	222	${}^{2_x}\bar{4}{}^{3_z}3{}^{2_x}m$	${}^{2_x}\bar{4}{}^{3_z}3{}^{2_x}m{}^{m_z}1$
432	222	${}^{2_x}4{}^{3_z}3{}^{2_x}2$	${}^{2_x}4{}^{3_z}3{}^{2_x}2{}^{m_z}1$
$4/m\bar{3}2/m$	mmm	${}^{2_x}4/{}^{1}m{}^{3_z}\bar{3}{}^{2_x}2/{}^{2_x}m$	${}^{2_x}4/{}^{1}m{}^{3_z}\bar{3}{}^{2_x}2/{}^{2_x}m{}^{m_z}1$

TABLE S10. Category-X SPGs of the form $G_{NSP} \times Z_2^K$, i.e., the types the spin part of which could be chosen as $G_{\mathrm{NSP}}^{s} = D_4$ and the direction $\boldsymbol{n}$ of which is parallel to the $\boldsymbol{z}$-axis is shown in this table. There are 5 types in total.

G_{p0}	N_{p0}	G_{NSP}	$G_{\mathrm{SP}} = G_{\mathrm{NSP}} \times Z_2^K$
422	1	${}^{4_z}4{}^{2_x}2{}^{2_{xy}}2$	${}^{4_z}4{}^{2_x}2{}^{2_{xy}}2{}^{m_z}1$
$4mm$	1	${}^{4_z}4{}^{2_x}2{}^{2_{xy}}2$	${}^{4_z}4{}^{2_x}2{}^{2_{xy}}2{}^{m_z}1$
$\bar{4}2m$	1	${}^{4_z}\bar{4}{}^{2_x}2{}^{2_{xy}}m$	${}^{4_z}\bar{4}{}^{2_x}2{}^{2_{xy}}m{}^{m_z}1$
$4/mmm$	m	${}^{4_z}4/{}^{1}m{}^{2_x}m{}^{2_{xy}}m$	${}^{4_z}4/{}^{1}m{}^{2_x}m{}^{2_{xy}}m{}^{m_z}1$

$4/mmm$	$\bar{1}$	${}^{4_z}4/{}^{2_z}m{}^{2_x}m{}^{2_{xy}}m$	${}^{4_z}4/{}^{2_z}m{}^{2_x}m{}^{2_{xy}}m^{m_z}1$

TABLE S11. Category-XI SPGs of the form $G_{NSP} \times Z_2^K$, i.e., the types the spin part of which could be chosen as $G_{NSP}^S = D_6$ and the direction $\boldsymbol{n}$ of which is parallel to the $\boldsymbol{z}$-axis is shown in this table. There are 8 types in total.

G_{p0}	N_{p0}	G_{NSP}	$G_{\mathrm{SP}} = G_{\mathrm{NSP}} \times Z_2^K$
$\bar{3}m$	1	${}^{6_z}\bar{3}^{2_x}m$	${}^{6_z}\bar{3}^{2_x}m^{m_z}1$
622	1	${}^{6_z}6^{2_x}2^{2_l}2$	${}^{6_z}6^{2_x}2^{2_l}2^{m_z}1$
$6mm$	1	${}^{6_z}6^{2_x}m^{2_l}m$	${}^{6_z}6^{2_x}m^{2_l}m^{m_z}1$
$\bar{6}m2$	1	${}^{6_z}\bar{6}^{2_x}m^{2_l}2$	${}^{6_z}\bar{6}^{2_x}m^{2_l}2^{m_z}1$
$6/mmm$	$\bar{1}$	${}^{6_z}6/{}^{2_z}m{}^{2_x}m{}^{2_l}m$	${}^{6_z}6/{}^{2_z}m{}^{2_x}m{}^{2_l}m^{m_z}1$
$6/mmm$	m	${}^{6_z}6/{}^{1}m{}^{2_x}m{}^{2_l}m$	${}^{6_z}6/{}^{1}m{}^{2_x}m{}^{2_l}m^{m_z}1$
$6/mmm$	2	${}^{3_z}6/{}^{2_z}m{}^{2_x}m{}^{2_{xy}}m$	${}^{3_z}6/{}^{2_z}m{}^{2_x}m{}^{2_{xy}}m^{m_z}1$
$4/m\bar{3}2/m$	222	${}^{2_2}4/{}^{2_z}m{}^{6_z}\bar{3}^{2_2}2/{}^{2_x}m$	${}^{2_2}4/{}^{2_z}m{}^{6_z}\bar{3}^{2_2}2/{}^{2_x}m^{m_z}1$

TABLE S12. 32 SPGs of the form $G_{NSP} \times \left(Z_2^K \ltimes SO(2)\right)$ with the corresponding G_{NSP}^S being C_1. The first column lists the G_{p0} corresponding to G_{NSP} shown in the second column. The third column lists all the types of SPGs of the form $G_{NSP} \times [Z_2^K \ltimes SO(2)]$ having G_{NSP} shown in the second column.

G_{p0}	G_{NSP}	$G_{SP} = G_{NSP} \times [Z_2^K \ltimes SO(2)]$
1	${}^{1}1$	${}^{\infty m}1$
$\bar{1}$	${}^{1}\bar{1}$	${}^{1}\bar{1}^{\infty m}1$
2	${}^{1}2$	${}^{1}2^{\infty m}1$
m	${}^{1}m$	${}^{1}m^{\infty m}1$
$2/m$	${}^{1}2/{}^{1}m$	${}^{1}2/{}^{1}m^{\infty m}1$
$mm2$	${}^{1}m{}^{1}m{}^{1}2$	${}^{1}m{}^{1}m{}^{1}2^{\infty m}1$
222	${}^{1}2{}^{1}2{}^{1}2$	${}^{1}2{}^{1}2{}^{1}2^{\infty m}1$
mmm	${}^{1}m{}^{1}m{}^{1}m$	${}^{1}m{}^{1}m{}^{1}m^{\infty m}1$
4	${}^{1}4$	${}^{1}4^{\infty m}1$
$\bar{4}$	${}^{1}\bar{4}$	${}^{1}\bar{4}^{\infty m}1$
$4/m$	${}^{1}4/{}^{1}m$	${}^{1}4/{}^{1}m^{\infty m}1$
422	${}^{1}4{}^{1}2{}^{1}2$	${}^{1}4{}^{1}2{}^{1}2^{\infty m}1$
$4mm$	${}^{1}4{}^{1}m{}^{1}m$	${}^{1}4{}^{1}m{}^{1}m^{\infty m}1$
$\bar{4}2m$	${}^{1}\bar{4}{}^{1}2{}^{1}m$	${}^{1}\bar{4}{}^{1}2{}^{1}m^{\infty m}1$
$4/mmm$	${}^{1}4/{}^{1}m{}^{1}m{}^{1}m$	${}^{1}4/{}^{1}m{}^{1}m{}^{1}m^{\infty m}1$

3	${}^{1}3$	${}^{1}3^{\infty m}1$
$\bar{3}$	${}^{1}\bar{3}$	${}^{1}\bar{3}^{\infty m}1$
32	${}^{1}3^{1}2$	${}^{1}3^{1}2^{\infty m}1$
$3m$	${}^{1}3^{1}m$	${}^{1}3^{1}m^{\infty m}1$
$\bar{3}m$	${}^{1}\bar{3}^{1}m$	${}^{1}\bar{3}^{1}m^{\infty m}1$
$\bar{6}$	${}^{1}\bar{6}$	${}^{1}\bar{6}^{\infty m}1$
6	${}^{1}6$	${}^{1}6^{\infty m}1$
622	${}^{1}6^{1}2^{1}2$	${}^{1}6^{1}2^{1}2^{\infty m}1$
$6/m$	${}^{1}6/{}^{1}m$	${}^{1}6/{}^{1}m^{\infty m}1$
$6mm$	${}^{1}6^{1}m^{1}m$	${}^{1}6^{1}m^{1}m^{\infty m}1$
$\bar{6}m2$	${}^{1}\bar{6}^{1}m^{1}2$	${}^{1}\bar{6}^{1}m^{1}2^{\infty m}1$
$6/mmm$	${}^{1}6/{}^{1}m^{1}m^{1}m$	${}^{1}6/{}^{1}m^{1}m^{1}m^{\infty m}1$
23	${}^{1}2^{1}3$	${}^{1}2^{1}3^{\infty m}1$
$2/m\bar{3}$	${}^{1}2/{}^{1}m^{1}\bar{3}$	${}^{1}2/{}^{1}m^{1}\bar{3}^{\infty m}1$
$\bar{4}3m$	${}^{1}\bar{4}^{1}3^{1}m$	${}^{1}\bar{4}^{1}3^{1}m^{\infty m}1$
432	${}^{1}4^{1}3^{1}2$	${}^{1}4^{1}3^{1}2^{\infty m}1$
$4/m\bar{3}2/m$	${}^{1}4/{}^{1}m^{1}\bar{3}^{1}2/{}^{1}m$	${}^{1}4/{}^{1}m^{1}\bar{3}^{1}2/{}^{1}m^{\infty m}1$

TABLE S13. 58 types of SPGs of the form $G_{NSP} \times [Z_2^K \ltimes SO(2)]$ the spin part of which could be chosen as $G_{NSP}^{s} = S_2 (= C_i = Z_2^T)$.

G_{p0}	G_{NSP}	$G_{SP} = G_{NSP} \times [Z_2^K \ltimes SO(2)]$
$\bar{1}$	${}^{\bar{1}}\bar{1}$	${}^{\bar{1}}\bar{1}^{\infty m}1$
2	${}^{\bar{1}}2$	${}^{\bar{1}}2^{\infty m}1$
m	${}^{\bar{1}}m$	${}^{\bar{1}}m^{\infty m}1$
$2/m$	${}^{1}2/{}^{\bar{1}}m$	${}^{1}2/{}^{\bar{1}}m^{\infty m}1$
$2/m$	${}^{\bar{1}}2/{}^{1}m$	${}^{\bar{1}}2/{}^{1}m^{\infty m}1$
$2/m$	${}^{\bar{1}}2/{}^{\bar{1}}m$	${}^{\bar{1}}2/{}^{\bar{1}}m^{\infty m}1$
$mm2$	${}^{\bar{1}}m^{\bar{1}}m^{1}2$	${}^{\bar{1}}m^{\bar{1}}m^{1}2^{\infty m}1$
$mm2$	${}^{1}m^{\bar{1}}m^{\bar{1}}2$	${}^{1}m^{\bar{1}}m^{\bar{1}}2^{\infty m}1$
222	${}^{1}2^{\bar{1}}2^{\bar{1}}2$	${}^{1}2^{\bar{1}}2^{\bar{1}}2^{\infty m}1$
mmm	${}^{1}m^{\bar{1}}m^{\bar{1}}m$	${}^{1}m^{\bar{1}}m^{\bar{1}}m^{\infty m}1$
mmm	${}^{1}m^{1}m^{\bar{1}}m$	${}^{1}m^{1}m^{\bar{1}}m^{\infty m}1$
mmm	${}^{\bar{1}}m^{\bar{1}}m^{\bar{1}}m$	${}^{\bar{1}}m^{\bar{1}}m^{\bar{1}}m^{\infty m}1$
4	${}^{\bar{1}}4$	${}^{\bar{1}}4^{\infty m}1$

$\bar{4}$	${}^{\bar{1}}\bar{4}$	${}^{\bar{1}}\bar{4}^{\infty m}1$
$4/m$	${}^{\bar{1}}4/{}^{1}m$	${}^{\bar{1}}4/{}^{1}m^{\infty m}1$
$4/m$	${}^{\bar{1}}4/{}^{\bar{1}}m$	${}^{\bar{1}}4/{}^{\bar{1}}m^{\infty m}1$
$4/m$	${}^{1}4/{}^{\bar{1}}m$	${}^{1}4/{}^{\bar{1}}m^{\infty m}1$
422	${}^{1}4{}^{\bar{1}}2{}^{\bar{1}}2$	${}^{1}4{}^{\bar{1}}2{}^{\bar{1}}2^{\infty m}1$
422	${}^{\bar{1}}4{}^{1}2{}^{\bar{1}}2$	${}^{\bar{1}}4{}^{1}2{}^{\bar{1}}2^{\infty m}1$
$4mm$	${}^{1}4{}^{\bar{1}}m{}^{\bar{1}}m$	${}^{1}4{}^{\bar{1}}m{}^{\bar{1}}m^{\infty m}1$
$4mm$	${}^{\bar{1}}4{}^{1}m{}^{\bar{1}}m$	${}^{\bar{1}}4{}^{1}m{}^{\bar{1}}m^{\infty m}1$
$\bar{4}2m$	${}^{1}\bar{4}{}^{\bar{1}}2{}^{\bar{1}}m$	${}^{1}\bar{4}{}^{\bar{1}}2{}^{\bar{1}}m^{\infty m}1$
$\bar{4}2m$	${}^{\bar{1}}\bar{4}{}^{\bar{1}}2{}^{1}m$	${}^{\bar{1}}\bar{4}{}^{\bar{1}}2{}^{1}m^{\infty m}1$
$\bar{4}2m$	${}^{\bar{1}}\bar{4}{}^{1}2{}^{\bar{1}}m$	${}^{\bar{1}}\bar{4}{}^{1}2{}^{\bar{1}}m^{\infty m}1$
$4/mmm$	${}^{\bar{1}}4/{}^{\bar{1}}m{}^{\bar{1}}m{}^{1}m$	${}^{\bar{1}}4/{}^{\bar{1}}m{}^{\bar{1}}m{}^{1}m^{\infty m}1$
$4/mmm$	${}^{1}4/{}^{\bar{1}}m{}^{1}m{}^{1}m$	${}^{1}4/{}^{\bar{1}}m{}^{1}m{}^{1}m^{\infty m}1$
$4/mmm$	${}^{\bar{1}}4/{}^{1}m{}^{1}m{}^{\bar{1}}m$	${}^{\bar{1}}4/{}^{1}m{}^{1}m{}^{\bar{1}}m^{\infty m}1$
$4/mmm$	${}^{1}4/{}^{1}m{}^{\bar{1}}m{}^{\bar{1}}m$	${}^{1}4/{}^{1}m{}^{\bar{1}}m{}^{\bar{1}}m^{\infty m}1$
$4/mmm$	${}^{1}4/{}^{\bar{1}}m{}^{\bar{1}}m{}^{\bar{1}}m$	${}^{1}4/{}^{\bar{1}}m{}^{\bar{1}}m{}^{\bar{1}}m^{\infty m}1$
$\bar{3}$	${}^{\bar{1}}\bar{3}$	${}^{\bar{1}}\bar{3}^{\infty m}1$
32	${}^{1}3{}^{\bar{1}}2$	${}^{1}3{}^{\bar{1}}2^{\infty m}1$
$3m$	${}^{1}3{}^{\bar{1}}m$	${}^{1}3{}^{\bar{1}}m^{\infty m}1$
$\bar{3}m$	${}^{1}\bar{3}{}^{\bar{1}}m$	${}^{1}\bar{3}{}^{\bar{1}}m^{\infty m}1$
$\bar{3}m$	${}^{\bar{1}}\bar{3}{}^{1}m$	${}^{\bar{1}}\bar{3}{}^{1}m^{\infty m}1$
$\bar{3}m$	${}^{\bar{1}}\bar{3}{}^{\bar{1}}m$	${}^{\bar{1}}\bar{3}{}^{\bar{1}}m^{\infty m}1$
$\bar{6}$	${}^{\bar{1}}\bar{6}$	${}^{\bar{1}}\bar{6}^{\infty m}1$
6	${}^{\bar{1}}6$	${}^{\bar{1}}6^{\infty m}1$
622	${}^{1}6{}^{\bar{1}}2{}^{\bar{1}}2$	${}^{1}6{}^{\bar{1}}2{}^{\bar{1}}2^{\infty m}1$
622	${}^{\bar{1}}6{}^{1}2{}^{\bar{1}}2$	${}^{\bar{1}}6{}^{1}2{}^{\bar{1}}2^{\infty m}1$
$6/m$	${}^{\bar{1}}6/{}^{\bar{1}}m$	${}^{\bar{1}}6/{}^{\bar{1}}m^{\infty m}1$
$6/m$	${}^{\bar{1}}6/{}^{1}m$	${}^{\bar{1}}6/{}^{1}m^{\infty m}1$
$6/m$	${}^{1}6/{}^{\bar{1}}m$	${}^{1}6/{}^{\bar{1}}m^{\infty m}1$
$6mm$	${}^{1}6{}^{\bar{1}}m{}^{\bar{1}}m$	${}^{1}6{}^{\bar{1}}m{}^{\bar{1}}m^{\infty m}1$
$6mm$	${}^{\bar{1}}6{}^{1}m{}^{\bar{1}}m$	${}^{\bar{1}}6{}^{1}m{}^{\bar{1}}m^{\infty m}1$
$\bar{6}m2$	${}^{1}\bar{6}{}^{\bar{1}}m{}^{\bar{1}}2$	${}^{1}\bar{6}{}^{\bar{1}}m{}^{\bar{1}}2^{\infty m}1$
$\bar{6}m2$	${}^{\bar{1}}\bar{6}{}^{1}m{}^{\bar{1}}2$	${}^{\bar{1}}\bar{6}{}^{1}m{}^{\bar{1}}2^{\infty m}1$
$\bar{6}m2$	${}^{\bar{1}}\bar{6}{}^{\bar{1}}m{}^{1}2$	${}^{\bar{1}}\bar{6}{}^{\bar{1}}m{}^{1}2^{\infty m}1$
$6/mmm$	${}^{\bar{1}}6/{}^{\bar{1}}m{}^{1}m{}^{\bar{1}}m$	${}^{\bar{1}}6/{}^{\bar{1}}m{}^{1}m{}^{\bar{1}}m^{\infty m}1$

$6/mmm$	${}^{\bar{1}}6/{}^{1}m{}^{\bar{1}}m{}^{1}m$	${}^{\bar{1}}6/{}^{1}m{}^{\bar{1}}m{}^{1}m{}^{\infty m}1$
$6/mmm$	${}^{1}6/{}^{1}m{}^{\bar{1}}m{}^{\bar{1}}m$	${}^{1}6/{}^{1}m{}^{\bar{1}}m{}^{\bar{1}}m{}^{\infty m}1$
$6/mmm$	${}^{1}6/{}^{\bar{1}}m{}^{1}m{}^{1}m$	${}^{1}6/{}^{\bar{1}}m{}^{1}m{}^{1}m{}^{\infty m}1$
$6/mmm$	${}^{1}6/{}^{\bar{1}}m{}^{\bar{1}}m{}^{\bar{1}}m$	${}^{1}6/{}^{\bar{1}}m{}^{\bar{1}}m{}^{\bar{1}}m{}^{\infty m}1$
$2/m\bar{3}$	${}^{1}2/{}^{\bar{1}}m{}^{\bar{1}}\bar{3}$	${}^{1}2/{}^{\bar{1}}m{}^{\bar{1}}\bar{3}{}^{\infty m}1$
$\bar{4}3m$	${}^{\bar{1}}\bar{4}{}^{1}3{}^{\bar{1}}m$	${}^{\bar{1}}\bar{4}{}^{1}3{}^{\bar{1}}m{}^{\infty m}1$
432	${}^{\bar{1}}4{}^{1}3{}^{\bar{1}}2$	${}^{\bar{1}}4{}^{1}3{}^{\bar{1}}2{}^{\infty m}1$
$4/m\bar{3}2/m$	${}^{\bar{1}}4/{}^{1}m{}^{1}\bar{3}{}^{\bar{1}}2/{}^{\bar{1}}m$	${}^{\bar{1}}4/{}^{1}m{}^{1}\bar{3}{}^{\bar{1}}2/{}^{\bar{1}}m{}^{\infty m}1$
$4/m\bar{3}2/m$	${}^{\bar{1}}4/{}^{\bar{1}}m{}^{\bar{1}}\bar{3}{}^{\bar{1}}2/{}^{1}m$	${}^{\bar{1}}4/{}^{\bar{1}}m{}^{\bar{1}}\bar{3}{}^{\bar{1}}2/{}^{1}m{}^{\infty m}1$
$4/m\bar{3}2/m$	${}^{1}4/{}^{\bar{1}}m{}^{\bar{1}}\bar{3}{}^{1}2/{}^{\bar{1}}m$	${}^{1}4/{}^{\bar{1}}m{}^{\bar{1}}\bar{3}{}^{1}2/{}^{\bar{1}}m{}^{\infty m}1$

V. SYMMETRY OF TIGHT-BINDING HAMILTONIANS ON PERIODIC KAGOME LATTICE

To better understand symmetry of tight-binding Hamiltonians on Kagome lattices shown in Fig. 3(a), we first derive all irreducible co-representations (co-reps) of little co-groups at high symmetry momenta K and M with generators of every co-rep summarized in Table S14 and S16. Character tables of maximally unitary subgroups of little co-groups at K and M are summarized in Table S18 and S21, respectively. The full correspondence among single-valued representations of nonmagnetic little co-group, co-reps of spin little co-group, and double-valued co-reps of magnetic little co-group at K and M are separately summarized in Table S15 and S17.

A. Single orbital model

We next consider a tight-binding Hamiltonian of periodic Kagome lattice shown in Fig. 3(a). There are three sites in one unit cell with one orbit per site and local magnetic moments at all sites. The magnetic order adopted here is the same as NCL2-AFM magnetic structure. The tight-binding Hamiltonian is written as follows:

$$H = \sum_{\alpha,\beta} \sum_{<\boldsymbol{R},i;\boldsymbol{R}',j>} t\, a^{\dagger}_{\boldsymbol{R},i,\alpha}\delta_{\alpha,\beta}a_{\boldsymbol{R}',j,\beta} + \sum_{\boldsymbol{R},\,i} a^{\dagger}_{\boldsymbol{R},i,\alpha}(\boldsymbol{S_i}\cdot\boldsymbol{\sigma})_{\alpha,\beta}a_{\boldsymbol{R},\,i,\,\beta}$$

$$+ \sum_{<\boldsymbol{R},i;\boldsymbol{R}',j>} \left(it_1\nu_{R,\,i;R'j}\right)a^{\dagger}_{\boldsymbol{R},\,i,\,\alpha}s_{z\,\alpha\beta}c_{\boldsymbol{R}',j,\beta}\,, \tag{S45}$$

where $\boldsymbol{R}$ and $\boldsymbol{R}'$ represent coordinates of unit cells, i and j label atomic sites ($i, j = 1,2,3$) and α and β are indices of spin $\alpha, \beta = \uparrow, \downarrow$. In this Hamiltonian, the first term includes nearest-neighbor hopping. The second term represents the effects of local magnetic moments with $\boldsymbol{\sigma} = (\sigma_x, \sigma_y, \sigma_z)$ denoting Pauli matrices. The third term represents the symmetry allowed effective SOC felt by electrons going from site $\boldsymbol{R}' + \boldsymbol{r}_j$ to $\boldsymbol{R} + \boldsymbol{r}_i$ [4]. The point group part of this structure is ${}^{3_z}6/{}^{1}m^{2_x}m^{2_{xy}}m^{m_z}1$ with generators being $\{U_{\boldsymbol{z}}(\frac{2\pi}{3})||C_{\boldsymbol{z}}(\frac{\pi}{3})\}, \{U_{\boldsymbol{x}}(\pi)\,||C_{\boldsymbol{x}}(\pi)\}, \{E|I\}, \{U_{\boldsymbol{z}}(\pi)T||I\}$. From Fig. 3(b-c), we see that before magnetic order is introduced, there is a 4-fold degenerate band and a 2-fold degenerate band at K. In contrast, after introducing magnetic order, the 4-fold degenerate band splits into a 2-fold degenerate band. Two 1-fold degenerate bands and the 2-fold degenerate band maintain their degeneracy. However, when considering magnetic group of this structure, $Cmm'm'$, there cannot be any 2-fold degeneracy at K point, which has little co-group $2'2'2$. To account for this degeneracy, we use spin group symmetry operations to implement $k \cdot p$ method at K.

In the framework of spin group, little co-group at K point is ${}^{\bar{6}_z}6/{}^{1}m^{2_x}m^{m_l}m$, with the generators being $\{U_{\boldsymbol{z}}(\frac{2\pi}{3})||C_{\boldsymbol{z}}(\frac{\pi}{3})I\}, \{U_{\boldsymbol{x}}(\pi)\,||C_{\boldsymbol{x}}(\pi)\}$ and $\{U_{\boldsymbol{z}}(\pi)T||I\}$. From this Kagome lattice, symmetry transformations on the atomic orbitals $|\varphi_{\boldsymbol{R},\,i}, \alpha\rangle = a^{\dagger}_{\boldsymbol{R},i,\alpha}|0\rangle$ could be obtained in the following:

$$\widehat{C_{\boldsymbol{z}}(\frac{\pi}{3})}|\varphi_{\boldsymbol{R},\,i}, \alpha\rangle = |\varphi_{\boldsymbol{R}',\,i+1}, \alpha\rangle, \tag{S46}$$

$$\hat{I}|\varphi_{\boldsymbol{R},i},\alpha\rangle = |\varphi_{\boldsymbol{R}',i},\alpha\rangle, \tag{S47}$$

$$\widehat{C_{\boldsymbol{x}}(\pi)}|\varphi_{\boldsymbol{R},i},\alpha\rangle = |\varphi_{\boldsymbol{R}',3-i},\alpha\rangle, \tag{S48}$$

$$\widehat{U_{\boldsymbol{n}}(\theta)}|\varphi_{\boldsymbol{R},i},\alpha\rangle = \sum_{\alpha} exp(-i\theta\boldsymbol{n}\cdot\frac{\boldsymbol{\sigma}}{2})_{\beta\alpha}|\varphi_{\boldsymbol{R},i},\alpha\rangle, \tag{S49}$$

$$\widehat{T}|\varphi_{\boldsymbol{R},i},\alpha\rangle = \sum_{\alpha} (-i\sigma_y K)_{\beta\alpha}|\varphi_{\boldsymbol{R},i},\alpha\rangle, \tag{S50}$$

where $\boldsymbol{R}'$ depends on the locations of transformed atomic sites.

It is easy to find the representation matrices of generators of little co-group at K with the Bloch basis $\{|\psi_{K,1},\uparrow\rangle, |\psi_{K,2},\uparrow\rangle, |\psi_{K,3},\uparrow\rangle, |\psi_{K,1},\downarrow\rangle, |\psi_{K,2},\downarrow\rangle, |\psi_{K,3},\downarrow\rangle\}$, where $|\psi_{K,i},\alpha\rangle \equiv \sum_{\boldsymbol{R}} e^{i\boldsymbol{K}\cdot(\boldsymbol{R}+\boldsymbol{r}_i)}|\varphi_{\boldsymbol{R},i},\alpha\rangle$ [5]:

$$R(\{U_{\boldsymbol{z}}(\frac{2\pi}{3})||C_{\boldsymbol{z}}(\frac{\pi}{3})I\}) = R(U_{\boldsymbol{z}}(\frac{2\pi}{3}))\otimes R(C_{\boldsymbol{z}}(\frac{\pi}{3})I) = exp(-i\frac{\pi}{3}\cdot\frac{\sigma_z}{2})\otimes\begin{pmatrix}0&1&0\\0&0&-1\\-1&0&0\end{pmatrix}, \tag{S51}$$

$$R(\{U_{\boldsymbol{x}}(\pi)\,||C_{\boldsymbol{x}}(\pi)\}) = R(U_{\boldsymbol{x}}(\pi))\otimes R(C_{\boldsymbol{x}}(\pi)) = exp(-i\frac{\pi}{2}\cdot\frac{\sigma_x}{2})\otimes\begin{pmatrix}0&1&0\\1&0&0\\0&0&1\end{pmatrix}, \tag{S52}$$

$$R(\{U_{2z}T||I\}) = -i\sigma_{\boldsymbol{y}}K\otimes\begin{pmatrix}1&0&0\\0&1&0\\0&0&1\end{pmatrix}. \tag{S53}$$

The corresponding character is shown in Table S19. Considering together with the character table of the maximal unitary subgroup of little co-group at K (Table S18), the single-orbital band representation is the direct sum of co-reps $K_3^s(1)\oplus K_4^s(1)\oplus 2K_6^s(2)$. This is consistent with the fact that when neglecting magnetic order, the induced band representation of representation $A_g(2)$ $(s, d_{x^2}, d_{y^2}, d_{z^2}, ...)$ of site point group mmm of Wyckoff position 3g at K are $K_1(2)\oplus K_5(4)$. According to Table S15, the correspondence between band representations of the nonmagnetic group and spin group is $K_1(2)\oplus K_5(4)$

$\rightarrow K_6^s(2) \oplus \left(K_3^s(1) \oplus K_4^s(1) \oplus K_6^s(2)\right)$. This is also consistent with the band splitting shown in Fig. 3 (b-c).

When considering magnetic group, there are two kinds of K points with different little co-groups. We choose one of them with higher symmetry to demonstrate the band splitting process. The magnetic group of this point is $2'2'2$. With this magnetic group, all energy levels should be nondegenerate, and the co-rep $K_3^s(2)$ will become reducible and be subduced to two co-reps, $(SM)\overline{LD}_3(1)$ and $(SM)\overline{LD}_4(1)$ of the magnetic little co-group $2'2'2$, while $K_3^s(1)$ and $K_4^s(1)$ separately corresponds to co-rep $(SM)\overline{LD}_4(1)$ and $(SM)\overline{LD}_3(1)$, summarized in Fig. 3 (d).

Similarly, we can also get the representation matrices of the generators of little co-group at M $(0, 1/2, 0)$, i.e., the spin group ${}^1m^{2_x}m^{2_x}m^{m_z}1$:

$$R(\{E||C_{\boldsymbol{z}}(\pi)\}) = \sigma_0 \otimes \begin{pmatrix} -1 & 0 & 0 \\ 0 & -1 & 0 \\ 0 & 0 & 1 \end{pmatrix}, \tag{S54}$$

$$R(\{U_{\boldsymbol{x}}(\pi)||C_{\boldsymbol{x}}(\pi)\}) = R\left(C_{\boldsymbol{x}}(\pi)\right) \otimes R\left(U_{\boldsymbol{x}}(\pi)\right) = exp(-i\pi \cdot \tfrac{\sigma_x}{2}) \otimes \begin{pmatrix} 0 & -1 & 0 \\ -1 & 0 & 0 \\ 0 & 0 & 1 \end{pmatrix}, \tag{S55}$$

$$R(\{E||I\}) = \sigma_0 \otimes \begin{pmatrix} -1 & 0 & 0 \\ 0 & -1 & 0 \\ 0 & 0 & 1 \end{pmatrix}, \tag{S56}$$

$$R(\{U_{\boldsymbol{z}}(\pi)T||E\}) = -i * exp(-i\pi \cdot \tfrac{\sigma_x}{2}) \sigma_{\boldsymbol{y}} K \otimes \begin{pmatrix} 1 & 0 & 0 \\ 0 & 1 & 0 \\ 0 & 0 & 1 \end{pmatrix}. \tag{S57}$$

From the character table of the little co-group at M (Table S21) and character of this representation (Table S22), we obtain that this representation could be written as the following direct sum of irreducible co-reps: $M_1^{s,+}(1) \oplus M_2^{s,+}(1) \oplus 2M_3^{s,-}(1) \oplus 2M_4^{s,-}(1)$. The correspondence among the representation of s orbital of nonmagnetic site

group, nonmagnetic little co-group, spin little co-group, and magnetic little co-group are listed in Table S23.

The complete set of co-reps of spin little co-groups at K and M are separately listed in Table S14 and S16. Their correspondences between the single-valued representations of nonmagnetic groups and double-valued co-reps of magnetic groups are separately listed in Tables S15 and S17.

We may also understand the energy band degeneracy using $k \cdot p$ method. By implementing $R(g)H(\boldsymbol{k})R(g)^{-1} = H(g\boldsymbol{k})$, we can find the $k \cdot p$ Hamiltonian, the elements of which up to 0th-order of $\boldsymbol{k}$ are shown in the following:

$$H = \begin{pmatrix} a_0 & a_1 + \mathrm{i}a_2 & -a_1 + \mathrm{i}a_2 & exp(-i\frac{\pi}{3})b_1 & b_2 & exp(i\frac{\pi}{3})b_2 \\ a_1 - \mathrm{i}a_2 & a_0 & -a_1 - \mathrm{i}a_2 & b_2 & exp(i\frac{\pi}{3})b_1 & exp(-i\frac{\pi}{3})b_2 \\ -a_1 - \mathrm{i}a_2 & -a_1 + \mathrm{i}a_2 & a_0 & exp(i\frac{\pi}{3})b_2 & exp(-i\frac{\pi}{3})b_2 & -b_1 \\ exp(i\frac{\pi}{3})b_1 & b_2 & exp(-i\frac{\pi}{3})b_2 & a_0 & a_1 - \mathrm{i}a_2 & -a_1 - \mathrm{i}a_2 \\ b_2 & exp(-i\frac{\pi}{3})b_1 & exp(i\frac{\pi}{3})b_2 & a_1 + \mathrm{i}a_2 & a_0 & -a_1 + \mathrm{i}a_2 \\ exp(-i\frac{\pi}{3})b_2 & exp(i\frac{\pi}{3})b_2 & -b_1 & -a_1 + \mathrm{i}a_2 & -a_1 - \mathrm{i}a_2 & a_0 \end{pmatrix}, \tag{S58}$$

with a_i and b_i being real parameters. By choosing an arbitrary set of parameters, numerical calculations show that this Hamiltonian has two 2-fold degenerate energy levels and two 1-fold degenerate energy levels, which is consistent with the tight-binding model and thus shows that spin group symmetry can account for the symmetry of this Hamiltonian.

Note: Interestingly, the terms proportional to a_2 can be accounted for by the effective SOC felt by electrons hopping between nearest-neighbor sites in Eq. (S45), which do not break spin group symmetry. This fact shows that certain approximated versions of SOC may not completely couple the spin and lattice degrees of freedom. In

addition, the terms proportional to b_i represent the effective magnetic field felt by electrons hopping between two sites and exerted by a third site.

To explicitly show this degeneracy, we use the eigenstates of $C_z(\frac{\pi}{3})I$ as basis so that the Hamiltonian is simplified to be:

$$H = \begin{pmatrix} c_1 & d_1 & 0 & 0 & 0 & 0 \\ d_1 & c_2 & 0 & 0 & 0 & 0 \\ 0 & 0 & c_1 & d_1 & 0 & 0 \\ 0 & 0 & d_1 & c_2 & 0 & 0 \\ 0 & 0 & 0 & 0 & c_3 & d_2 \\ 0 & 0 & 0 & 0 & d_2 & c_3 \end{pmatrix}, \tag{S59}$$

which shows a block-diagonalized form with three blocks. The first 2 blocks are identical and have two different eigenvalues in general, contributing to two 2-fold degenerate energy levels. The third block also has two different eigenvalues and thus contributes to two 1-fold degenerate energy levels.

The spin group ${}^{\bar{6}_z}6/{}^1m^{2_x}m^{m_l}m$ is isomorphic to magnetic point group $6'/mmm'$ up to spin rotations. However, the co-reps of ${}^{\bar{6}_z}6/{}^1m^{2_x}m^{m_l}m$ listed above is different from either single-valued co-reps or double-valued co-reps of $6'/mmm'$. This is because in ${}^{\bar{6}_z}6/{}^1m^{2_x}m^{m_l}m$, when spatial rotation is 2π, the accompanied spin rotation could be either odd multiples or even multiples of 2π.

B. p orbital model

For the lattice in Fig. 3(a), we consider another model with 3 atomic orbitals, including p_x, p_y and p_z, at each site. The tight-binding Hamiltonian is written as follows:

$$H = \sum_{\alpha,\beta,\mu,\nu} \Big(\sum_{R,i} \Delta_\lambda \, \delta_{\alpha,\beta} a^\dagger_{R,i,\mu,\alpha} R^i_{\mu,\lambda} (R^i_{\lambda,\nu})^T a_{R',i,\nu,\beta} + \sum_{<R,i;R',j>} t^{i,j}_{\mu,\nu} \delta_{\alpha,\beta} a^\dagger_{R,i,\mu,\alpha} a_{R',j,\nu,\beta}$$

$$+\sum_{R,\,i}\delta_{\mu,\nu}a^{\dagger}_{R,i,\mu,\alpha}(\boldsymbol{S}_i\cdot\boldsymbol{\sigma})_{\alpha,\beta}a_{R,\,i,\nu,\beta}\Big), \tag{S60}$$

where $\boldsymbol{R}$ and $\boldsymbol{R}'$ represent coordinates of unit cells, i and j label atomic sites ($i,j=1,2,3$), μ, ν and λ label p orbitals ($\mu,\nu,\lambda=x,y,z$), and α and β are indices of spin ($\alpha,\beta=\uparrow,\downarrow$). In this equation, the first term considers onsite crystal field splitting, the second term is the hopping term between nearest neighbors, and the third term includes onsite magnetic moments. $R^i_{\lambda,\nu}$ is the rotation matrix that rotates p_x, p_y and p_z of the global frame into the local frame of site-i, with the form $R^i=\begin{bmatrix} Cos(2(i-1)\pi/3) & -Sin(2(i-1)\pi/3) & 0\\ Sin(2(i-1)\pi/3) & Cos(2(i-1)\pi/3) & 0\\ 0 & 0 & 1\end{bmatrix}$. $\Delta_\lambda$is the onsite energy of local p_λ orbital. $t_{\mu,\nu}$ are hopping amplitude between p orbitals of nearest neighbor dependent on two Slater-Koster parameters, including $V_{pp\pi}$ and $V_{pp\sigma}$, and direction cosines of vectors connecting two neighboring sites, e.g., $t^{i,j}_{x,x}=l^2V_{pp\sigma}+(1-l^2)V_{pp\pi}$ with $l=(\boldsymbol{r}_i-\boldsymbol{r}_j)\cdot\hat{\boldsymbol{x}}/|\boldsymbol{r}_i-\boldsymbol{r}_j|$, $t^{i,j}_{x,y}=lmV_{pp\sigma}-lmV_{pp\pi}$ with $l=(\boldsymbol{r}_i-\boldsymbol{r}_j)\cdot\hat{\boldsymbol{x}}/|\boldsymbol{r}_i-\boldsymbol{r}_j|$ and $m=(\boldsymbol{r}_i-\boldsymbol{r}_j)\cdot\hat{\boldsymbol{y}}/|\boldsymbol{r}_i-\boldsymbol{r}_j|$, etc.

Our calculation results are summarized in Fig. S2. Interestingly, in this case, the 18 bands of the model can be viewed as 3 sets of bands, with each obtained from a single orbital model. Before the magnetic order is turned on, there are three four-fold degenerate states and two 2-fold degenerate states at K (Fig. S2 (b)). After adding the magnetic term, every four-fold degenerate state splits into one two-fold degenerate state and two nondegenerate states (Fig. S2 (c)). Since the site symmetry of the lattice is reduced to *mmm,* that breaks the isotropy between p_x and p_y orbitals, as shown in Fig. S2 (b-c), the energy bands are allowed to be decomposed into three bundles, which are dominated by p_x, p_y and p_z orbitals, respectively.

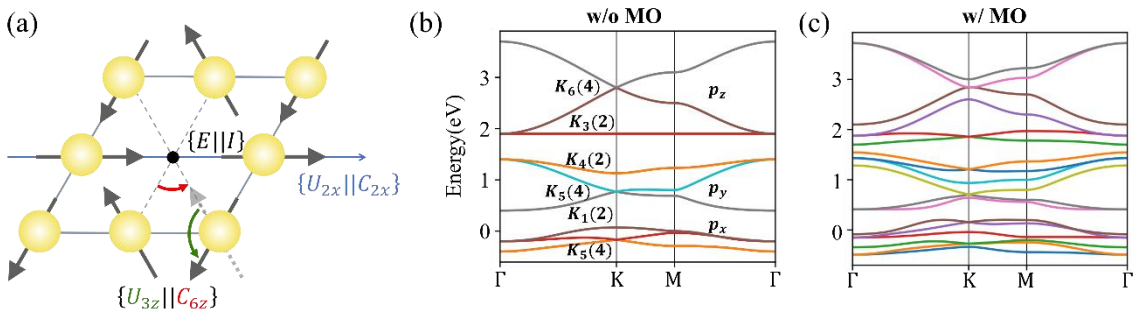

Fig. S2. Calculation results of a spinful kagome lattice with noncolinear AFM spin configuration shown in (a) and with three orbitals, including p_x, p_y and p_z per site. (b-c) SOC-free band structure of the kagome lattice without (b) and with (c) magnetic order, with onsite crystal field splitting, Slater-Koster parameters, and magnetic term in (S64) set to be $(\Delta_x, \Delta_y, \Delta_z)$=$(0.0, 0.9, 2.5)$, $(V_{pp\sigma}, V_{pp\pi}) = (0.1, 0.3)$ and $|\boldsymbol{S}_i| = 0$ (without magnetic order) or 0.17 (with magnetic order).

We next derive the band representations of this model following similar procedures as those of section VA. By representing the atomic orbitals as $|\varphi_{\boldsymbol{R},i,\mu},\alpha\rangle = a^{\dagger}_{R,i,\mu,\alpha}|0\rangle$, actions of different operations on these states could be obtained in the following:

$$\widehat{C_{\boldsymbol{z}}(\frac{\pi}{3})}|\varphi_{\boldsymbol{R},i,\mu},\alpha\rangle = \sum_{\nu=x,y,z}|\varphi_{\boldsymbol{R}',i+1,\nu},\alpha\rangle exp(-i\frac{\pi}{3}L_z{}^{l=1})_{\nu\mu}\,, \tag{S61}$$

$$\hat{I}|\varphi_{\boldsymbol{R},i,\mu},\alpha\rangle = -|\varphi_{\boldsymbol{R}',i,\mu},\alpha\rangle, \tag{S62}$$

$$\widehat{C_{\boldsymbol{x}}(\pi)}|\varphi_{\boldsymbol{R},i,\mu},\alpha\rangle = \sum_{\nu=x,y,z}|\varphi_{\boldsymbol{R}',3-i,\nu},\alpha\rangle exp(-i\pi L_x{}^{l=1})_{\nu\mu}, \tag{S63}$$

$$\widehat{U_{\boldsymbol{n}}(\theta)}|\varphi_{\boldsymbol{R},i,\mu},\alpha\rangle = \sum_{\alpha} exp(-i\theta\boldsymbol{n}\cdot\frac{\boldsymbol{\sigma}}{2})_{\beta\alpha}|\varphi_{\boldsymbol{R},i,\mu},\alpha\rangle, \tag{S64}$$

$$\widehat{T}|\varphi_{\boldsymbol{R},i,\mu},\alpha\rangle = \sum_{\alpha}(-i\sigma_y K)_{\beta\alpha}|\varphi_{\boldsymbol{R},i,\mu},\alpha\rangle, \tag{S65}$$

where $L_z{}^{l=1}$ and $L_x{}^{l=1}$ are representation matrices of angular momentum operator with

the basis of real p orbitals. ${L_z}^{l=1} = \begin{pmatrix} 0 & -i & 0 \\ i & 0 & 0 \\ 0 & 0 & 0 \end{pmatrix}$, ${L_x}^{l=1} = \begin{pmatrix} 0 & 0 & 0 \\ 0 & 0 & -i \\ 0 & i & 0 \end{pmatrix}$. Thus, we can write the representation matrices of generators of little co-group of K, i.e., the group ${}^{\bar{6}_z}6/{}^1m^{2_x}m^{m_l}m$, on the Bloch basis $|\psi_{\boldsymbol{K},1,\,x},\uparrow\rangle, |\psi_{\boldsymbol{K},1,\,y},\uparrow\rangle, |\psi_{\boldsymbol{K},1,\,z},\uparrow\rangle, |\psi_{\boldsymbol{K},2,\,x},\uparrow\rangle, |\psi_{\boldsymbol{K},2,\,y},\uparrow\rangle,$ $|\psi_{\boldsymbol{K},2,\,z},\uparrow\rangle, |\psi_{\boldsymbol{K},3,\,x},\uparrow\rangle, |\psi_{\boldsymbol{K},3,y},\uparrow\rangle, |\psi_{\boldsymbol{K},3,\,z},\uparrow\rangle, |\psi_{\boldsymbol{K},1,\,x},\downarrow\rangle, |\psi_{\boldsymbol{K},1,\,y},\downarrow\rangle, |\psi_{\boldsymbol{K},1,\,z},\downarrow\rangle, |\psi_{\boldsymbol{K},2,x},\downarrow\rangle,$ $|\psi_{\boldsymbol{K},2,y},\downarrow\rangle, |\psi_{\boldsymbol{K},2,\,z},\downarrow\rangle, |\psi_{\boldsymbol{K},3,\,x},\downarrow\rangle, |\psi_{\boldsymbol{K},3,\,y},\downarrow\rangle|\psi_{\boldsymbol{K},3,z},\downarrow\rangle\}$, where $|\psi_{\boldsymbol{K},\boldsymbol{i},\mu},\alpha\rangle \equiv \sum_{\boldsymbol{R}} e^{i\boldsymbol{K}\cdot(\boldsymbol{R}+\boldsymbol{r}_i)}|\varphi_{\boldsymbol{R},\,i,\mu},\alpha\rangle$:

$$R\left(\{U_{\boldsymbol{z}}(\tfrac{2\pi}{3})||C_{\boldsymbol{z}}(\tfrac{\pi}{3})I\}\right) = R\left(U_{\boldsymbol{z}}(\tfrac{2\pi}{3})\right)\otimes R\left(C_{\boldsymbol{z}}(\tfrac{\pi}{3})I\right)$$

$$= exp(-i\tfrac{2\pi}{3}\cdot\tfrac{\sigma_z}{2})\otimes\begin{pmatrix} 0 & 0 & 1 \\ -1 & 0 & 0 \\ 0 & 1 & 0 \end{pmatrix}\otimes exp(-i\tfrac{\pi}{3}{L_z}^{l=1}), \tag{S66}$$

$$R(\{U_{\boldsymbol{x}}(\pi)||C_{\boldsymbol{x}}(\pi)\}) = R\big(C_{\boldsymbol{x}}(\pi)\big)\otimes R\big(U_{\boldsymbol{x}}(\pi)\big)$$

$$= exp(-i\pi\cdot\tfrac{\sigma_x}{2})\otimes\begin{pmatrix} 0 & 1 & 0 \\ 1 & 0 & 0 \\ 0 & 0 & 1 \end{pmatrix}\otimes exp(-i\pi{L_x}^{l=1}), \tag{S67}$$

$$R(\{U_{\boldsymbol{x}}(\pi)T||I\}) = -i\sigma_y K\otimes\begin{pmatrix} 1 & 0 & 0 \\ 0 & 1 & 0 \\ 0 & 0 & 1 \end{pmatrix}\otimes\begin{pmatrix} -1 & 0 & 0 \\ 0 & -1 & 0 \\ 0 & 0 & -1 \end{pmatrix}. \tag{S68}$$

The corresponding character is shown in Table S19. Considering together with the character table of the little co-group of K (Table S18), the *p*-orbital band representation is the direct sum of co-reps $K_1^s(1)\oplus K_2^s(1)\oplus 2K_3^s(1)\oplus 2K_4^s(1)\oplus 2K_5^s(2)\oplus 4K_6^s(2)$. The decomposition can be understood in the following. When the magnetic order is neglected, the Wyckoff positions (3g) of the Kagome lattice have the site point group mmm, indicating the anisotropy among each of p_x, p_y and p_z orbitals. Therefore, the induced band representations of B_{1u} (p_z orbital), B_{2u} (p_x orbital) and B_{3u} (p_y orbital) for

the little co-group representation of K give rise to $K_3(2)\oplus K_6(4)$, $K_4(2)\oplus K_5(4)$ and $K_1(2)\oplus K_5(4)$, respectively. According to Table S15, the correspondence between band representations of nonmagnetic group and spin group are:

$$K_3(2)\oplus K_6(4) \to K_5^s(2) \oplus \left(K_1^s(1) \oplus K_2^s(1) \oplus K_5^s(2)\right),$$

$$K_4(2)\oplus K_5(4) \to K_6^s(2) \oplus \left(K_3^s(1) \oplus K_4^s(1) \oplus K_6^s(2)\right),$$

$$K_1(2)\oplus K_5(4) \to K_6^s(2) \oplus \left(K_3^s(1) \oplus K_4^s(1) \oplus K_6^s(2)\right),$$

consistent with the band splitting shown in Fig. S2. The correspondences among the representations of nonmagnetic site group, nonmagnetic little co-group, spin little co-group, and magnetic little co-group are listed in Table S20.

Similarly, we can also write the representation matrices of the generators of little co-group at M $(0, 1/2, 0)$, i.e., the spin group ${}^1m^{2_x}m^{2_x}m^{m_z}1$:

$$R(\{E||C_{\boldsymbol{z}}(\pi)\}) = \sigma_0 \otimes \begin{pmatrix} -1 & 0 & 0 \\ 0 & -1 & 0 \\ 0 & 0 & 1 \end{pmatrix} \otimes exp(-i\pi {L_z}^{l=1}), \tag{S69}$$

$$R(\{U_{\boldsymbol{x}}(\pi)||C_{\boldsymbol{x}}(\pi)\}) = R\left(C_{\boldsymbol{x}}(\pi)\right) \otimes R\left(U_{\boldsymbol{x}}(\pi)\right)$$

$$= exp(-i\pi \cdot \tfrac{\sigma_x}{2}) \otimes \begin{pmatrix} 0 & -1 & 0 \\ -1 & 0 & 0 \\ 0 & 0 & 1 \end{pmatrix} \otimes exp(-i\pi {L_x}^{l=1}), \tag{S70}$$

$$R(\{E||I\}) = \sigma_0 \otimes \begin{pmatrix} -1 & 0 & 0 \\ 0 & -1 & 0 \\ 0 & 0 & 1 \end{pmatrix} \otimes \begin{pmatrix} -1 & 0 & 0 \\ 0 & -1 & 0 \\ 0 & 0 & -1 \end{pmatrix}, \tag{S71}$$

$$R(\{U_{\boldsymbol{z}}(\pi)T||E\}) = -i * exp(-i\pi \cdot \tfrac{\sigma_x}{2}) \sigma_y K \otimes \begin{pmatrix} 1 & 0 & 0 \\ 0 & 1 & 0 \\ 0 & 0 & 1 \end{pmatrix} \otimes \begin{pmatrix} 1 & 0 & 0 \\ 0 & 1 & 0 \\ 0 & 0 & 1 \end{pmatrix}. \tag{S72}$$

From the character table of the little co-group at M (Table S21) and the character of the *p*-orbital representation (Table S22), we obtain the decomposition of irreducible co-reps: $4M_1^{s,+}(1) \oplus M_1^{s,-}(1) \oplus 4M_2^{s,+}(1) \oplus M_2^{s,-}(1) \oplus 2M_3^{s,+}(1) \oplus 2M_3^{s,-}(1) \oplus$

$2M_4^{s,+}(1) \oplus 2M_4^{s,-}(1)$. The correspondence between the representations of site group, nonmagnetic group, spin group, and magnetic group are listed in Table S23.

TABLE S14. The list of representation matrices (with complex conjugation) of spin little co-group at K.

${}^{\bar{6}_z}6/{}^1m^{2_x}m^{m_l}m$	$\{U_{\boldsymbol{z}}(\frac{2\pi}{3})\|\|C_{\boldsymbol{z}}(\frac{\pi}{3})I\}$	$\{U_{\boldsymbol{x}}(\pi)\|\|C_{\boldsymbol{x}}(\pi)\}$	$\{U_{\boldsymbol{z}}(\pi)T\|\|I\}$
$K_1^s(1)$	1	i	K
$K_2^s(1)$	1	$-i$	K
$K_3^s(1)$	-1	i	K
$K_4^s(1)$	-1	$-i$	K
$K_5^s(2)$	$\begin{pmatrix} exp(-i\frac{2\pi}{3}) & 0 \\ 0 & exp(i\frac{2\pi}{3}) \end{pmatrix}$	$\begin{pmatrix} 0 & -i \\ -i & 0 \end{pmatrix}$	$\begin{pmatrix} 0 & 1 \\ 1 & 0 \end{pmatrix}K$
$K_6^s(2)$	$\begin{pmatrix} exp(i\frac{\pi}{3}) & 0 \\ 0 & exp(-i\frac{\pi}{3}) \end{pmatrix}$	$\begin{pmatrix} 0 & -i \\ -i & 0 \end{pmatrix}$	$\begin{pmatrix} 0 & 1 \\ 1 & 0 \end{pmatrix}K$

TABLE S15. Correspondence among single-valued representations of nonmagnetic group, co-reps of spin group, and double-valued co-reps of magnetic group at K. The number in the parenthesis denotes degeneracy including spin. Note: in the framework of magnetic group, K points are no longer high symmetry points. There are two kinds of K points

distinguished by their little co-groups, with one of them along SM line (u,0,0) with little co-group $2'2'2$ and the other on P plane (u,v,0) with little co-group $2'$. The representations of nonmagnetic and magnetic groups are obtained from Bilbao Crystallographic Server (https://cryst.ehu.es/) [6,7].

Nonmagnetic group	Spin group	Magnetic group	
$\bar{6}m2 \times SO(3) \times Z_2^T$	${}^{\bar{6}_z}6/{}^{1}m^{2_x}m^{m_l}m$	$2'2'2$	$2'$
$K_1(2)$	$K_6^s(2)$	$(SM)\overline{LD}_4(1)$	$(P)\overline{GP}_2(1)$
		$(SM)\overline{LD}_3(1)$	$(P)\overline{GP}_2(1)$
$K_2(2)$	$K_5^s(2)$	$(SM)\overline{LD}_4(1)$	$(P)\overline{GP}_2(1)$
		$(SM)\overline{LD}_3(1)$	$(P)\overline{GP}_2(1)$
$K_3(2)$	$K_5^s(2)$	$(SM)\overline{LD}_4(1)$	$(P)\overline{GP}_2(1)$
		$(SM)\overline{LD}_3(1)$	$(P)\overline{GP}_2(1)$
$K_4(2)$	$K_6^s(2)$	$(SM)\overline{LD}_4(1)$	$(P)\overline{GP}_2(1)$
		$(SM)\overline{LD}_3(1)$	$(P)\overline{GP}_2(1)$
$K_5(4)$	$K_3^s(1)$	$(SM)\overline{LD}_4(1)$	$(P)\overline{GP}_2(1)$
	$K_4^s(1)$	$(SM)\overline{LD}_3(1)$	$(P)\overline{GP}_2(1)$
	$K_6^s(2)$	$(SM)\overline{LD}_4(1)$	$(P)\overline{GP}_2(1)$
		$(SM)\overline{LD}_3(1)$	$(P)\overline{GP}_2(1)$

$K_6(4)$	$K_1^s(1)$	$(SM)\overline{LD}_4(1)$	$(P)\overline{GP}_2(1)$
	$K_2^s(1)$	$(SM)\overline{LD}_3(1)$	$(P)\overline{GP}_2(1)$
	$K_5^s(2)$	$(SM)\overline{LD}_4(1)$	$(P)\overline{GP}_2(1)$
		$(SM)\overline{LD}_3(1)$	$(P)\overline{GP}_2(1)$

TABLE S16. The list of representation matrices (with complex conjugation) of spin little groups at M.

${}^1m^{2_x}m^{2_x}m^{m_z}1$	$\{E\|\|C_z(\pi)\}$	$\{U_x(\pi)\ \|\|C_x(\pi)\}$	$\{E\|\|I\}$	$\{U_z(\pi)T\|\|E\}$
$M_1^{s,+}(1)$	1	$-i$	1	K
$M_1^{s,-}(1)$	1	$-i$	-1	K
$M_2^{s,+}(1)$	1	i	1	K
$M_2^{s,-}(1)$	1	i	-1	K
$M_3^{s,+}(1)$	-1	$-i$	1	K
$M_3^{s,-}(1)$	-1	$-i$	-1	K
$M_4^{s,+}(1)$	-1	i	1	K
$M_4^{s,-}(1)$	-1	i	-1	K

TABLE S17. Correspondence among single-valued representations of nonmagnetic group, co-reps of spin group, and double-valued co-reps of magnetic group at M. The number in the parenthesis denotes degeneracy including spin. Note: in the framework of magnetic

group, there are two kinds of M points distinguished by their little co-groups, with one of them is folded to Γ point (0,0,0) with little co-group $\mathrm{m}'m'\mathrm{m}$ while the other is at S point (-1/2,1/2,0) with little co-group $2'/m'$.

Nonmagnetic group	Spin group	Magnetic group	
$mmm \times SO(3) \times Z_2^T$	${}^1m^{2_x}m^{2_x}m^{m_z}1$	$m'm'm$	$2'/m'$
$M_1^+(2)$	$M_1^{s,+}(1)$	$\overline{GM}_3(1)$	$(S)\overline{V}_3(1)$
	$M_2^{s,+}(1)$	$\overline{GM}_4(1)$	$(S)\overline{V}_3(1)$
$M_1^-(2)$	$M_1^{s,-}(1)$	$\overline{GM}_5(1)$	$(S)\overline{V}_2(1)$
	$M_2^{s,-}(1)$	$\overline{GM}_6(1)$	$(S)\overline{V}_2(1)$
$M_2^+(2)$	$M_1^{s,+}(1)$	$\overline{GM}_3(1)$	$(S)\overline{V}_3(1)$
	$M_2^{s,+}(1)$	$\overline{GM}_4(1)$	$(S)\overline{V}_3(1)$
$M_2^-(2)$	$M_1^{s,-}(1)$	$\overline{GM}_5(1)$	$(S)\overline{V}_2(1)$
	$M_2^{s,-}(1)$	$\overline{GM}_6(1)$	$(S)\overline{V}_2(1)$
$M_3^+(2)$	$M_3^{s,+}(1)$	$\overline{GM}_3(1)$	$(S)\overline{V}_3(1)$
	$M_4^{s,+}(1)$	$\overline{GM}_4(1)$	$(S)\overline{V}_3(1)$
$M_3^-(2)$	$M_3^{s,-}(1)$	$\overline{GM}_5(1)$	$(S)\overline{V}_2(1)$
	$M_4^{s,-}(1)$	$\overline{GM}_6(1)$	$(S)\overline{V}_2(1)$
$M_4^+(2)$	$M_3^{s,+}(1)$	$\overline{GM}_3(1)$	$(S)\overline{V}_3(1)$

	$M_4^{s,+}(1)$	$\overline{GM}_4(1)$	$(S)\overline{V}_3(1)$
$M_4^-(2)$	$M_3^{s,-}(1)$	$\overline{GM}_5(1)$	$(S)\overline{V}_2(1)$
	$M_4^{s,-}(1)$	$\overline{GM}_6(1)$	$(S)\overline{V}_2(1)$

TABLE S18. The character table for the maximal unitary subgroup (MUSG) of little co-group at K, i.e., for subgroup ${}^{3_z}\bar{6}^{2_x}m^{2_{xy}}2$ of ${}^{\bar{6}_z}6/{}^{1}m^{2_x}m^{m_l}m$, where C_i are conjugate classes:

C_1: $\{E||E\}$,

C_2: $\{U_{\boldsymbol{x}_0}(\pi)||C_{\boldsymbol{x}_0}(\pi)\}, \{U_{\boldsymbol{x}_4}(\pi)||C_{\boldsymbol{x}_2}(\pi)\}, \{U_{\boldsymbol{x}_2}(\pi)||C_{\boldsymbol{x}_4}(\pi)\}$,

C_3: $\{U_{\boldsymbol{x}_2}(\pi)||C_{\boldsymbol{x}_1}(\pi)I\}, \{U_{\boldsymbol{x}_0}(\pi)||C_{\boldsymbol{x}_3}(\pi)I\}, \{U_{\boldsymbol{x}_4}(\pi)||C_{\boldsymbol{x}_5}(\pi)I\}$,

C_4: $\{U_{\boldsymbol{z}}(\frac{2\pi}{3})||C_{\boldsymbol{z}}(\frac{\pi}{3})I\}, \{U_{\boldsymbol{z}}(\frac{10\pi}{3})||C_{\boldsymbol{z}}(\frac{5\pi}{3})I\}$,

C_5: $\{U_{\boldsymbol{z}}(\frac{4\pi}{3})||C_{\boldsymbol{z}}(\frac{2\pi}{3})I\}, \{U_{\boldsymbol{z}}(\frac{8\pi}{3})||C_{\boldsymbol{z}}(\frac{4\pi}{3})I\}$,

C_6: $\{U_{\boldsymbol{z}}(2\pi)||C_{\boldsymbol{z}}(\pi)I\}$,

where the rotation axes are $\boldsymbol{x}_n = cos(n\pi/6)\boldsymbol{x} + sin(n\pi/6)\boldsymbol{y}, n = 0,1,\ldots,5$.

	C_1	C_2	C_3	C_4	C_5	C_6
$K_1^s(1)$	1	i	i	1	1	1
$K_2^s(1)$	1	$-i$	$-i$	1	1	1
$K_3^s(1)$	1	i	$-i$	-1	1	-1
$K_4^s(1)$	1	$-i$	i	-1	1	-1
$K_5^s(2)$	2	0	0	-1	-1	2
$K_6^s(2)$	2	0	0	1	-1	-2

TABLE S19. The character table for the band representations of *s*-orbital model and *p*-orbital model of subgroup ${}^{3_z}\bar{6}^{2_x}m^{2_{xy}}2$ of little co-group ${}^{\bar{6}_z}6/{}^{1}m^{2_x}m^{m_l}m$ at K.

	C_1	C_2	C_3	C_4	C_5	C_6
single orbital $K_3^s(1) \oplus K_4^s(1)$ $\oplus\ 2K_6^s(2)$	6	0	0	0	0	-6
p orbital $K_1^s(1) \oplus K_2^s(1)$ $\oplus\ 2K_1^s(1) \oplus 2K_2^s(1)$ $\oplus\ 2K_5^s(2) \oplus 4K_6^s(2)$	18	0	0	0	0	-6

TABLE S20. The correspondence among single-valued representations of nonmagnetic site symmetry group mmm at Wyckoff position 3g, single-valued representations of the nonmagnetic group, co-reps of spin group, and double-valued co-reps of magnetic group at K. The number in the parenthesis denotes degeneracy, including spin.

Real space	Reciprocal space			
Nonmagnetic site symmetry group	Nonmagnetic little co-group at K	Spin group at K	Magnetic group at K	
mmm	$\bar{6}m2 \times SO(3) \times Z_2^T$	${}^{\bar{6}_z}6/{}^{1}m^{2_x}m^{m_l}m$	$2'2'2$	$2'$
$A_g(2)$ $(s, d_{x^2}, d_{y^2},$	$K_1(2)$	$K_6^s(2)$	$(SM)\overline{LD}_4(1)$	$(P)\overline{GP}_2(1)$
			$(SM)\overline{LD}_3(1)$	$(P)\overline{GP}_2(1)$
	$K_5(4)$	$K_3^s(1)$	$(SM)\overline{LD}_4(1)$	$(P)\overline{GP}_2(1)$

d_{z^2}, …)		$K_4^s(1)$	$(SM)\overline{LD}_3(1)$	$(P)\overline{GP}_2(1)$
		$K_6^s(2)$	$(SM)\overline{LD}_4(1)$	$(P)\overline{GP}_2(1)$
			$(SM)\overline{LD}_3(1)$	$(P)\overline{GP}_2(1)$
	$K_3(2)$	$K_5^s(2)$	$(SM)\overline{LD}_4(1)$	$(P)\overline{GP}_2(1)$
			$(SM)\overline{LD}_3(1)$	$(P)\overline{GP}_2(1)$
$B_{1u}(2)$	$K_6(4)$	$K_1^s(1)$	$(SM)\overline{LD}_4(1)$	$(P)\overline{GP}_2(1)$
$(p_z$, …)		$K_2^s(1)$	$(SM)\overline{LD}_3(1)$	$(P)\overline{GP}_2(1)$
		$K_5^s(2)$	$(SM)\overline{LD}_4(1)$	$(P)\overline{GP}_2(1)$
			$(SM)\overline{LD}_3(1)$	$(P)\overline{GP}_2(1)$
	$K_4(2)$	$K_6^s(2)$	$(SM)\overline{LD}_4(1)$	$(P)\overline{GP}_2(1)$
			$(SM)\overline{LD}_3(1)$	$(P)\overline{GP}_2(1)$
$B_{2u}(2)$	$K_5(4)$	$K_3^s(1)$	$(SM)\overline{LD}_4(1)$	$(P)\overline{GP}_2(1)$
$(p_y$, …)		$K_4^s(1)$	$(SM)\overline{LD}_3(1)$	$(P)\overline{GP}_2(1)$
		$K_6^s(2)$	$(SM)\overline{LD}_4(1)$	$(P)\overline{GP}_2(1)$
			$(SM)\overline{LD}_3(1)$	$(P)\overline{GP}_2(1)$
	$K_1(2)$	$K_6^s(2)$	$(SM)\overline{LD}_4(1)$	$(P)\overline{GP}_2(1)$
			$(SM)\overline{LD}_3(1)$	$(P)\overline{GP}_2(1)$
$B_{3u}(2)$	$K_5(4)$	$K_3^s(1)$	$(SM)\overline{LD}_4(1)$	$(P)\overline{GP}_2(1)$
$(p_x$, …)		$K_4^s(1)$	$(SM)\overline{LD}_3(1)$	$(P)\overline{GP}_2(1)$
		$K_6^s(2)$	$(SM)\overline{LD}_4(1)$	$(P)\overline{GP}_2(1)$
			$(SM)\overline{LD}_3(1)$	$(P)\overline{GP}_2(1)$

TABLE S21. The character table for the maximal unitary subgroups (MUSGs) of little co-group at M (0, 1/2, 0), i.e., for subgroup ${}^{1}m^{2}m^{2}m$ of ${}^{1}m^{2_x}m^{2_x}m^{m_z}1$, where C_i are conjugate classes:

C_1: $\{E||E\}$, C_2: $\{E||C_z(\pi)\}$, C_3: $\{U_x(\pi)||C_y(\pi)\}$, C_4: $\{U_x(\pi)||C_x(\pi)\}$, C_5: $\{E||I\}$,

C_6: $\{E||C_z(\pi)I\}$, C_7: $\{U_x(\pi)||C_y(\pi)I\}$, C_8: $\{U_x(\pi)||C_x(\pi)I\}$

	C_1	C_2	C_3	C_4	C_5	C_6	C_7	C_8
$M_1^{s,+}(1)$	1	1	$-i$	$-i$	1	1	$-i$	$-i$
$M_1^{s,-}(1)$	1	1	$-i$	$-i$	-1	-1	i	i
$M_2^{s,+}(1)$	1	1	i	i	1	1	i	i
$M_2^{s,-}(1)$	1	1	i	i	-1	-1	$-i$	$-i$
$M_3^{s,+}(1)$	1	-1	i	$-i$	1	-1	i	$-i$
$M_3^{s,-}(1)$	1	-1	i	$-i$	-1	1	$-i$	i
$M_4^{s,+}(1)$	1	-1	$-i$	i	1	-1	$-i$	i
$M_4^{s,-}(1)$	1	-1	$-i$	i	-1	1	i	$-i$

TABLE S22. The character table for the band representations of single orbital model and p orbital model of subgroup ${}^{1}m^{2}m^{2}m$ of little co-group ${}^{1}m^{2_x}m^{2_x}m^{m_z}1$ at M.

	C_1	C_2	C_3	C_4	C_5	C_6	C_7	C_8
single orbital $M_1^{s,+}(1) \oplus M_2^{s,+}(1) \oplus 2M_3^{s,-}(1)$ $\oplus 2M_4^{s,-}(1)$	6	-2	0	0	-2	6	0	0
p orbital $4M_1^{s,+}(1) \oplus M_1^{s,-}(1) \oplus 4M_2^{s,+}(1)$	18	2	0	0	6	6	0	0

$\oplus M_2^{s,-}(1) \oplus 2M_3^{s,+}(1) \oplus 2M_3^{s,-}(1)$ $\oplus 2M_4^{s,+}(1) \oplus 2M_4^{s,-}(1)$								

TABLE S23. The correspondence among single-valued representations of nonmagnetic site symmetry group mmm at Wyckoff position 3g, single-valued representations of nonmagnetic group, co-reps of the spin group, and double-valued co-reps of magnetic group at M, which are induced by single-valued representations of nonmagnetic site symmetry group mmm at Wyckoff position 3g. The number in the parenthesis denotes degeneracy, including spin.

Real space	Reciprocal space			
Nonmagnetic site symmetry group at 3g	Nonmagnetic little co-group at M	Spin group at M	Magnetic group at M	
mmm	$mmm \times SO(3) \times Z_2^T$	${}^1m^{2_x}m^{2_x}m^{m_z}1$	$m'm'm$	$2'/m'$
$A_g(2)$ (s, d_{x2}, d_{y2}, d_{z2}, …)	$M_1^+(2)$	$M_1^{s,+}(1)$	$\overline{GM}_3(1)$	$(S)\overline{V}_3(1)$
		$M_2^{s,+}(1)$	$\overline{GM}_4(1)$	$(S)\overline{V}_3(1)$
	$M_3^-(2)$	$M_3^{s,-}(1)$	$\overline{GM}_5(1)$	$(S)\overline{V}_2(1)$
		$M_4^{s,-}(1)$	$\overline{GM}_6(1)$	$(S)\overline{V}_2(1)$
	$M_4^-(2)$	$M_3^{s,-}(1)$	$\overline{GM}_5(1)$	$(S)\overline{V}_2(1)$
		$M_4^{s,-}(1)$	$\overline{GM}_6(1)$	$(S)\overline{V}_2(1)$
$B_{1u}(2)$ (p_z, …)	$M_2^-(2)$	$M_1^{s,-}(1)$	$\overline{GM}_5(1)$	$(S)\overline{V}_2(1)$
		$M_2^{s,-}(1)$	$\overline{GM}_6(1)$	$(S)\overline{V}_2(1)$

	$M_3^+(2)$	$M_3^{s,+}(1)$	$\overline{GM}_3(1)$	$(S)\overline{V}_3(1)$
		$M_4^{s,+}(1)$	$\overline{GM}_4(1)$	$(S)\overline{V}_3(1)$
	$M_4^+(2)$	$M_3^{s,+}(1)$	$\overline{GM}_3(1)$	$(S)\overline{V}_3(1)$
		$M_4^{s,+}(1)$	$\overline{GM}_4(1)$	$(S)\overline{V}_3(1)$
$B_{2u}(2)$ $(p_y, \ldots)$	$M_1^+(2)$	$M_1^{s,+}(1)$	$\overline{GM}_3(1)$	$(S)\overline{V}_3(1)$
		$M_2^{s,+}(1)$	$\overline{GM}_4(1)$	$(S)\overline{V}_3(1)$
	$M_2^+(2)$	$M_1^{s,+}(1)$	$\overline{GM}_3(1)$	$(S)\overline{V}_3(1)$
		$M_2^{s,+}(1)$	$\overline{GM}_4(1)$	$(S)\overline{V}_3(1)$
	$M_4^-(2)$	$M_3^{s,-}(1)$	$\overline{GM}_5(1)$	$(S)\overline{V}_2(1)$
		$M_4^{s,-}(1)$	$\overline{GM}_6(1)$	$(S)\overline{V}_2(1)$
$B_{3u}(2)$ $(p_x, \ldots)$	$M_1^+(2)$	$M_1^{s,+}(1)$	$\overline{GM}_3(1)$	$(S)\overline{V}_3(1)$
		$M_2^{s,+}(1)$	$\overline{GM}_4(1)$	$(S)\overline{V}_3(1)$
	$M_2^+(2)$	$M_1^{s,+}(1)$	$\overline{GM}_3(1)$	$(S)\overline{V}_3(1)$
		$M_2^{s,+}(1)$	$\overline{GM}_4(1)$	$(S)\overline{V}_3(1)$
	$M_3^-(2)$	$M_3^{s,-}(1)$	$\overline{GM}_5(1)$	$(S)\overline{V}_2(1)$
		$M_4^{s,-}(1)$	$\overline{GM}_6(1)$	$(S)\overline{V}_2(1)$

VI. CONSTRUCTION AND TOPOLOGICAL ASPECTS OF A TIGHT-BINDING HAMILTONIAN WITH Z_2 TOPOLOGICAL PHASES

First, to facilitate implementing Table I of the main text in tight-binding models obtained from atomic orbitals [$|\varphi_{\boldsymbol{R},i,\mu},\alpha\rangle$] ($\boldsymbol{R}$ – coordinates of unit cells; i – label of

atomic sites; μ – label of orbitals at a site; α – label of spin), we write general matrix representations of the symmetry operators with the basis of Bloch wavefunctions Fourier-transformed from $|\varphi_{\boldsymbol{R},\,i,\mu},\alpha\rangle$, defined as $|\psi_{\boldsymbol{k},i,\mu},\alpha\rangle \equiv \sum_{\boldsymbol{R}} e^{i\boldsymbol{k}\cdot(\boldsymbol{R}+\boldsymbol{r}_i)}|\varphi_{\boldsymbol{R},\,i,\mu},\alpha\rangle$ [5]:

$$R(T) = -i\sigma_y K;\, R\big(U_{\boldsymbol{n}}(\pi)\big) = e^{-i\pi\,\boldsymbol{n}\cdot\frac{\boldsymbol{\sigma}}{2}};\, R_{\boldsymbol{k}}(\tau_{\boldsymbol{n}/2}) = e^{-i\frac{\boldsymbol{n}\cdot\boldsymbol{k}}{2}}\rho_x;$$

$$R\big(C_{\boldsymbol{n}}(\pi)\big) = \oplus_w\,[\,M^w(C_{\boldsymbol{n}}(\pi))\otimes[\,\oplus_{N=1,2,\ldots}\,[\,\oplus_{l=0}^{N}\,[e^{-i\pi\,\boldsymbol{n}\cdot\boldsymbol{L}^l}\,]]\,];$$

$$R(m_{\boldsymbol{n}}) = \oplus_w\,[\,M^w(m_{\boldsymbol{n}})\otimes[\,\oplus_{N=1,2,\ldots}\,[\,\oplus_{l=0}^{N}\,[e^{-i\pi\,\boldsymbol{n}\cdot\boldsymbol{L}^l}Q^l(I)\,]]\,];$$

where the indices are defined by: w – index of Wyckoff positions in a crystal; N – principal quantum number; l – azimuthal quantum number; ρ_x – the first Pauli matrix that switches two sublattices connected by $\tau_{\boldsymbol{n}/2}$.

$M^w(C_{\boldsymbol{n}}(\pi))$ and $M^w(m_{\boldsymbol{n}})$ are representation matrices of $C_{\boldsymbol{n}}(\pi)$ and $m_{\boldsymbol{n}}$ with the basis of a set of atoms labeled by a Wyckoff position. $\boldsymbol{L}^l$ and $Q^l(I)$ in $R(C_{\boldsymbol{n}}(\pi))/R(m_{\boldsymbol{n}})$ separately stands for the representation matrix of angular momentum and inversion operator with the basis of a set of Wannier functions of azimuthal quantum number l (possibly from different atomic sites), connected by $C_n(\pi)/m_n$ symmetry. Note: since a symmetry operation could transform $|\psi_{\boldsymbol{k},i,\mu},\alpha\rangle$ into $|\psi_{\boldsymbol{k}+\boldsymbol{K},j,\nu},\beta\rangle$ where $\boldsymbol{K}$ is a reciprocal lattice vector, there might be a phase factor in M^w if we consider $|\psi_{\boldsymbol{k},j,\nu},\beta\rangle$ rather than $|\psi_{\boldsymbol{k}+\boldsymbol{K},j,\nu},\beta\rangle$ as the basis vector.

Then, we show how we construct models with nontrivial Z_2 topological phases protected by spin group symmetry.

In magnetic materials without SOC, we find that spin group includes two additional symmetry operations that could protect Z_2 topological phases, except for $\{T||E|0\}$ and $\{T||E|\tau_{\boldsymbol{z}/2}\}$ that separately appears in nonmagnetic materials and magnetic materials with

SOC. One of them is $\{TU_{\boldsymbol{n}}(\pi)||E|\tau_{\boldsymbol{z}/2}\}$ symmetry, which has $\{\widehat{TU_{\boldsymbol{n}}(\pi)||E|\tau_{\boldsymbol{z}/2}}\}^2 = -1$ with the basis of Bloch states on $k_z = \pi$ plane in the Brillouin Zone. This symmetry also transforms Hamiltonians at $k_z = \pi$ plane like two-dimensional (2D) time reversal symmetry, i.e., $\{\widehat{TU_{\boldsymbol{n}}(\pi)||E|\tau_{\boldsymbol{z}/2}}\}H(k_x, k_y, \pi)\{\widehat{TU_{\boldsymbol{n}}(\pi)||E|\tau_{1/2}^{\boldsymbol{z}}}\}^{-1} = H(-k_x, -k_y, \pi)$. Then, it is evident that $\{TU_{\boldsymbol{n}}(\pi)||E|\tau_{\boldsymbol{z}/2}\}$ symmetry allows Z_2 classification at $k_z = \pi$ plane, similar to the Z_2 classification at $k_z = 0$ plane protected by $\{T||E|\tau_{\boldsymbol{z}/2}\}$ symmetry. Furthermore, $\{TU_{\boldsymbol{n}}(\pi)||E|\tau_{\boldsymbol{z}/2}\}$ symmetry is unbroken on side surfaces parallel to $\tau_{1/2}^{\boldsymbol{z}}$, which is also similar to the case of $\{T||E|\tau_{\boldsymbol{z}/2}\}$ symmetry, thus the Z_2 topological phases protected by $\{TU_{\boldsymbol{n}}(\pi)||E|\tau_{\boldsymbol{z}/2}\}$ symmetry would have gapless Dirac cone surface states on side surfaces.

Another symmetry operation is $\{T||m_{[001]}|0\}$, which has $\{T||\widehat{m_{[001]}}|0\}^2 = -1$ with the basis of Bloch states with arbitrary momenta in the Brillouin Zone. Furthermore, it transforms the Hamiltonian as 2D time reversal symmetry at any plane parallel to the mirror plane of $m_{[001]}$, i.e., $\{T||\widehat{m_{[001]}}|0\}\widehat{H}(k_x, k_y, k_z)\{T||\widehat{m_{[001]}}|0\}^{-1} = \widehat{H}(-k_x, -k_y, k_z)$. Thus, $\{T||m_{[001]}|0\}$ allows Z_2 topological classifications at every plane parallel to the mirror plane of $m_{[001]}$. Similar to $\{TU_{\boldsymbol{n}}(\pi)||E|\tau_{\boldsymbol{z}/2}\}$, $\{T||m_{[001]}|0\}$ is also preserved on side surfaces perpendicular to the mirror plane and thus protects gapless surface states on side surfaces. Furthermore, if one of the 2D planes parallel to the mirror plane in momentum space has Z_2 invariant being 1 and the system is gaped in the whole Brillouin zone, then every plane parallel to the mirror plane has Z_2 invariant being 1 because topological invariants cannot be continuously changed. The gapless Dirac surface states corresponding to these planes will connect to form nodal-line Dirac surface

states on the side surfaces.

To realize topological insulators protected by $\{T||m_{[001]}|0\}$ symmetry and $\{TU_{\boldsymbol{n}}(\pi)||E|\tau_{\boldsymbol{z}/2}\}$ symmetry, we consider constructing a tight-binding model from known models and add magnetic order to change symmetries. To realize topological insulators protected by $\{T||m_{[001]}|0\}$ symmetry, we need every plane parallel to $m_{[001]}$ being topological nontrivial, which reminds us of Weyl semimetal since it generally has every plane between two Weyl points of opposite chirality being Chern insulators. To realize those protected by $\{TU_{\boldsymbol{n}}(\pi)||E|\tau_{\boldsymbol{z}/2}\}$, we may add A-type anti-ferromagnetism to nonmagnetic but topological nontrivial models to realize such phase. This process involves cell doubling and the length of the Brillouin zone along $\tau_{\boldsymbol{z}/2}$ would be reduced by half. We need the reduced Brillouin zone to have Z_2=1 for the 2D system on $k_z = \pi$ plane. This requires that the unreduced Brillouin zone should have the 2D system on $k_z = \pi/2$ plane being topological nontrivial. This analysis also leads us to Weyl semimetal. Thus, we start with a two-band and 3-dimensional Weyl semimetal model without SOC and magnetic order, given in Ref. [8], to construct a model that realizes the Z_2 topological phases protected by both $\{T||m_{[001]}|0\}$ symmetry and $\{TU_{\boldsymbol{n}}(\pi)||E|\tau_{\boldsymbol{z}/2}\}$ symmetry.

The resulting 8-band model Hamiltonian is shown as follows:

$$\begin{aligned}\mathcal{H}(\boldsymbol{k}) = \big[&2t\,Sin\,(\boldsymbol{k}\cdot\boldsymbol{a}_+)\tau_z\rho_x + 2t\,Sin\,(\boldsymbol{k}\cdot\boldsymbol{a}_-)\tau_0\rho_y \\ &+ \big[\Delta - 2t'[\,Cos\,(\boldsymbol{k}\cdot\boldsymbol{a}_x) + Cos\,(\boldsymbol{k}\cdot\boldsymbol{a}_y)\,]\big]\tau_0\rho_z \\ &+ 2t_\perp\,Cos\,(\boldsymbol{k}\cdot\frac{\boldsymbol{a}_z}{2})\;\tau_x\rho_z\big]\sigma_0 \\ &+ \tau^1\rho_0\boldsymbol{S_1}\cdot\boldsymbol{\sigma} + \tau^2\rho_0\boldsymbol{S_2}\cdot\boldsymbol{\sigma},\end{aligned} \tag{S73}$$

where $\boldsymbol{\tau} = (\tau_x, \tau_y, \tau_z), \boldsymbol{\rho} = (\rho_x, \rho_y, \rho_z)$ and $\boldsymbol{\sigma} = (\sigma_x, \sigma_y, \sigma_z)$ denote Pauli matrices acting

on layer, site, and spin degrees of freedom, and $\tau^1 = (\tau_0 + \tau_z)/2$, $\tau^2 = (\tau_0 - \tau_z)/2$. $\boldsymbol{S_1}$ and $\boldsymbol{S_2}$ denote the exchange field induced by local magnetic moments added on the two layers. $\boldsymbol{a_{x,y,z}}$ are three lattice vectors. $\boldsymbol{a}_+$ and $\boldsymbol{a}_-$ are the vectors pointing from A site to B site in the unit cell, $\boldsymbol{a}_\pm = (\boldsymbol{a}_x \pm \boldsymbol{a}_y)/2$.

This process of constructing Z_2 topological insulators can be viewed from the flow chart shown in Fig. S3. Starting with the two-band model in the Weyl semimetal phase, which has a layered structure, we firstly include spin degrees of freedom so that the Weyl points become 4-fold degenerate Dirac points. We then consider two models with opposite local magnetic moments (and opposite magnetic flux). The local magnetic moments split energy bands and thus give us two Weyl semimetals separately having two Weyl points if the occupation number is 1 or 3. The first Weyl semimetal has Chern number $C = +1$ on planes between two Weyl points, while the second Weyl semimetal has $C = -1$. We adjust the parameters such that $C \neq 0$ in $k_z = \pi/2$ plane.

Then we stack these two Weyl semimetals to construct a superlattice structure, or in other words, to add A-type AFM order to the original model. Because the directions of both magnetic moments and magnetic flux are opposite on the two layers, we have $\{T||I|0\}$, $\{T||E|\tau_{\boldsymbol{z}/2}\}$, $\{T||m_{[001]}|0\}$ and $\{TU_{\boldsymbol{z}}(\pi)||E|\tau_{\boldsymbol{z}/2}\}$ symmetry. Then, every band is two-fold degenerate because of the presence of $\{T||I|0\}$ symmetry, and thus two Weyl points with opposite chirality should combine to form a Dirac point giving rise to 2 Dirac points. Nevertheless, in reality, such Dirac points do not exist because the two Dirac points are annihilated with each other and leave fully gapped energy bands.

The phase of the resulting model is a topological insulator with $Z_2 = 1$ at $k_z = \chi$ plane for all $\chi \in (-\pi, \pi]$, thusis a combination of infinite number of topological phases

of 2D planes $k_z = \chi$. Such phase is protected by $\{T||E|\tau_{z/2}\}$, $\{T||m_{[001]}|0\}$ and $\{TU_z(\pi)||E|\tau_{z/2}\}$ symmetry at the same time, with Z_2 topological phase at $k_z = \pi$ protected by $\{TU_z(\pi)||E|\tau_{z/2}\}$ and $\{T||m_{[001]}|0\}$ symmetry, $k_z = 0$ protected by $\{T||E|\tau_{z/2}\}$ and $\{T||m_{[001]}|0\}$ symmetry, and Z_2 topological phases at $k_z = \chi$ for $\chi \neq \pi$ and $\chi \neq 0$ protected by $\{T||m_{[001]}|0\}$ symmetry. Because of the protection of $\{T||m_{[001]}|0\}$ symmetry, the surface states on side surface form gapless nodal line shown in Fig. 4(e).

If we slightly tilt the direction of two opposite magnetic moments so that they have the same tilted components in the x-y plane, both $\{T||E|\tau_{z/2}\}$ and $\{T||m_{[001]}|0\}$ will be broken and $\{TU_z(\pi)||E|\tau_{z/2}\}$ is the only symmetry left that could protect Z_2 topological phases. Thus, the surface states of the resulting Hamiltonian are gapped everywhere except for $k_z = \pi$, which constitute Dirac cone surface states, shown in Fig. 4(f). If we additionally pair two neighbor layers, then $\{TU_z(\pi)||E|\tau_{z/2}\}$ is also broken, so our calculation results in Fig. 4(h) show fully gapped surface states.

To further characterize the Z_2 topological phases protected by $\{T||m_{[001]}|0\}$ symmetry, we conducted Wilson loop calculations for topological trivial and nontrivial phases protected by $\{T||m_{[001]}|0\}$ (Fig. S5). The calculations are done by separately summing over Wannier centers of states in two subspaces connected by $\{T||m_{[001]}|0\}$ below Fermi level of topological trivial and nontrivial phases shown in Fig. S5 (a) and (d). Note that different from the Wilson loop of mirror Chern insulators, Wilson loops of Z_2 topological insulators are not gauge invariant. This is because, to calculate states projected onto subspaces, we must first select a subspace $|\varphi_k\rangle$ and then obtain another

subspace by operating symmetry $\{T||m_{[001]}|0\}$ on it $\{T||m_{[001]}|0\}|\varphi_{\boldsymbol{k}}\rangle$. Different $|\varphi_{\boldsymbol{k}}\rangle$ may have different Chern numbers and contribute to different Wilson loops. But the Chern number of different $|\varphi_{\boldsymbol{k}}\rangle$ should be differing by multiple of 2 due to the Z_2 nature of our topological insulator. To fix $|\varphi_{\boldsymbol{k}}\rangle$, we add a constant τ_z term to Eq. (S73), which causes a slight difference between onsite energies of nearby layers. This term causes spin splitting over the whole $k_z = 0$ plane because both $\{T||m_{[001]}|0\}$ and $\{T||I|0\}$ are slightly broken. Then we define $|\varphi_{\boldsymbol{k}}\rangle$ as energetically lower bands of every pair of spin-split bands. This gives rise to a smooth curve of the Wilson loop. The calculations of Wilson loop at $k_z = 0$ plane for both topological trivial and nontrivial phases are shown in Fig. S5 (b) and (e). For both topological trivial and nontrivial phases, Wilson loops obtained at $k_z = \nu\ (-\pi < \nu \leq \pi)$ are similar to the loop at $k_z = 0$ and thus is not illustrated here. The consistency between Wilson loop and surface states further shows that the Dirac nodal line surface states and the corresponding Z_2 topological nontrivial phase is indeed protected by $\{T||m_{[001]}|0\}$ symmetry.

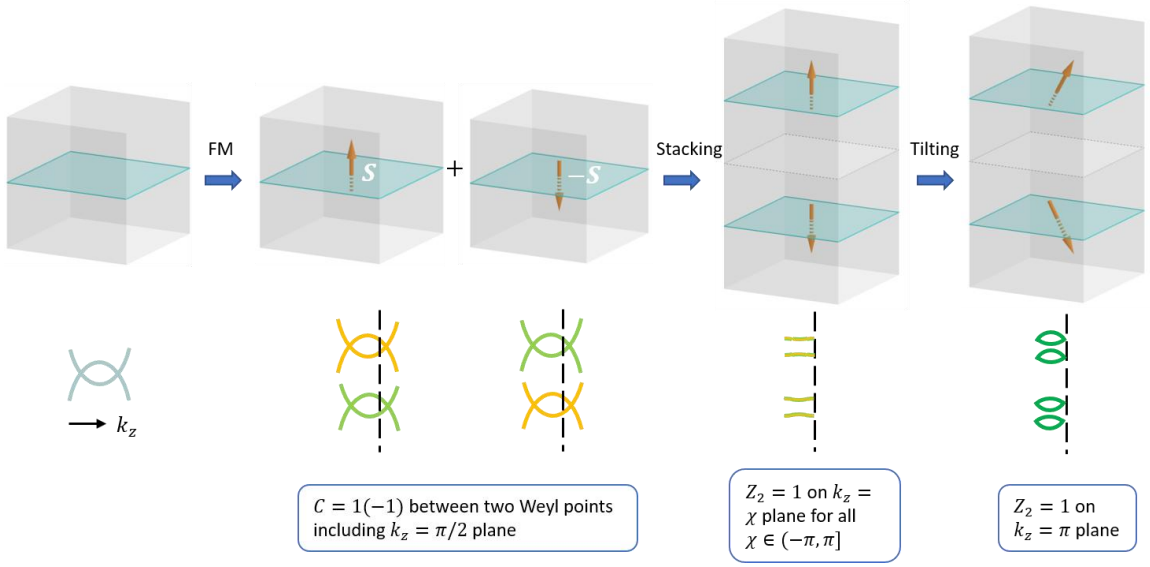

FIG. S3. Flow chart of construction of Z_2 topological insulators protected by $\{T||m_{[001]}|0\}$ and $\{TU_{\boldsymbol{n}}(\pi)||E|\tau_{\boldsymbol{z}/2}\}$ symmetry. The first row represents the magnetic orders and crystal structures of different steps, with the arrows representing local magnetic moments. The second row shows the diagram of corresponding band structures. The third row states the topological properties of different steps. FM represents an addition of ferromagnetism to the nonmagnetic model.

VII. TOPOLOGICAL PROPERTIES OF $AMnBi_2$ (A = Sr, Ca) FROM THE PERSPECTIVE OF SPIN GROUP SYMMETRY

The magnetic square net materials $AMnBi_2$ (A = Sr, Ca) were previously thought to be Dirac semimetals when neglecting SOC. However, the symmetry properties of these materials and the relationship between symmetry and topological properties have not been discussed because a complete framework for analyzing magnetic materials without SOC is not used previously.

Without magnetic order, $SrMnBi_2$ and $CaMnBi_2$ separately have space groups $I4/mmm$ and $P4/nmm$. In the framework of spin group, if neglecting magnetic order, the symmetry groups are $I4/mmm \otimes O^s(3)$ and $P4/mmm \otimes O^s(3)$. Using the notation in Section IV, the point groups corresponding to these two groups are both ${}^14/{}^1m{}^1m{}^1m \otimes O^s(3)$. Ref. [9] uses a nonmagnetic tight-binding model to show the following two statements. First, without Sr or Ca atom, the tight-binding model is a nodal line semimetal, with a nodal line located in $k_z = 0$ plane because of the band folding effect. Second, with Sr atoms, the nodal line is mostly gapped except for the crossing at the $M - \Gamma$ line, while with Ca atoms, the nodal line is not gapped at all. This is attributed to

the differences of next-nearest-neighbor hopping between $SrMnBi_2$ and $CaMnBi_2$. However, DFT calculations of $SrMnBi_2$ and $CaMnBi_2$ show that both $CaMnBi_2$ and $SrMnBi_2$ are Dirac semimetal. The deviation between model calculation and DFT calculation is because (1) the model used does not include magnetic order, and (2) the model is two-dimensional rather than three-dimensional.

Because of the difference between spin group symmetry of magnetic and nonmagnetic cases, the tight-binding Hamiltonian has not accurately accounted for the topological properties. Without magnetic order, both $SrMnBi_2$ and $CaMnBi_2$ have inversion symmetry $\{E||I|0\}$ and thus crossings between two bands should be nodal lines in general [10]. This can be seen by using a 4-band model Hamiltonian and implementing $\{T||I|0\}$ symmetry and full spin rotation symmetry group $SO(3)$ to restrict such Hamiltonian. By representing $\{T||I|0\}$ and $\{U_{\boldsymbol{n}}(\theta)||E|0\}$ as $\tau_x(-i\sigma_y)K$ and $exp(-i\theta \boldsymbol{n}\cdot\frac{\boldsymbol{\sigma}}{2})$, we can see that the resulting Hamiltonian is of the form

$$H(\boldsymbol{k}) = f_0(\boldsymbol{k})\sigma_0\tau_0 + f_1(\boldsymbol{k})\sigma_0\tau_x + f_2(\boldsymbol{k})\sigma_0\tau_y. \tag{S74}$$

This Hamiltonian contains no Pauli matrix acting on spin space because of the spin rotation symmetry group $SO(3)$. Moreover, additional implementation of $\{T||I|0\}$ leaves 3 terms in the Hamiltonian, with the first term proportional to identity matrix and the last 2 terms anticommuting with each other. So, the crossing between two bands requires that the last two terms are zero at the same time, which gives 2 equations of 3 parameters (k_x, k_y, k_z). Thus, if these equations have solutions, the solutions should form a line in general, except for the point nodes resulting from high dimensional representations at high symmetry momenta.

However, our result is still inconsistent with the nonmagnetic tight-binding model,

where $SrMnBi_2$ is shown to be a Dirac semimetal rather than a nodal line semimetal. This is because the tight-binding Hamiltonian used is two-dimensional rather than three-dimensional. If including a third dimension, the Hamiltonian for $SrMnBi_2$ will show a nodal line semimetal with nodal lines directing along the third dimension.

The above analysis shows why nonmagnetic 3D materials with inversion symmetry should generally have band crossings as Dirac nodal lines rather than Dirac points and accounts for 2D nonmagnetic tight-binding models that lead to the results in Ref. [9].

However, there is no nodal line in magnetic $AMnBi_2$ (A = Sr, Ca). This is because, without full spin operation, we could only implement $\{U_{\boldsymbol{z}}(\theta)||E|0\}$ and $\{T||I|0\}$ symmetry to constrain a 4-band Hamiltonian in general, resulting the Hamiltonian of the following form

$$H(\boldsymbol{k}) = f_0(\boldsymbol{k})\sigma_0\tau_0 + f_1(\boldsymbol{k})\sigma_0\tau_x + f_2(\boldsymbol{k})\sigma_0\tau_y + f_3(\boldsymbol{k})\sigma_z\tau_z. \tag{S75}$$

This model Hamiltonian has one more term than the nonmagnetic Hamiltonian in Eq. (S74), so crossings of bands are generally Dirac nodal points rather than Dirac nodal lines. Furthermore, the mirror symmetry is also broken because of the presence of magnetic order. The only additional symmetry that possibly protects nodal lines is the combination of mirror symmetry (glide mirror symmetry) and spin rotation for $SrMnBi_2$ ($CaMnBi_2$), i.e., $\{U_{\boldsymbol{x}}(\pi)||m_{\boldsymbol{z}}|0\}$ ($\{U_{\boldsymbol{x}}(\pi)||m_{\boldsymbol{z}}|\tau_{\boldsymbol{xy}/2}\}$). However, it is easy to show that their eigenvalues are switched by $\{T||I|0\}$ symmetry, leading to two different mirror eigenvalues embedded in every two-fold degenerate band. Thus, the combined symmetry of spin rotation and (glide) mirror will not provide additional protection, and nodal lines cannot be created in general.

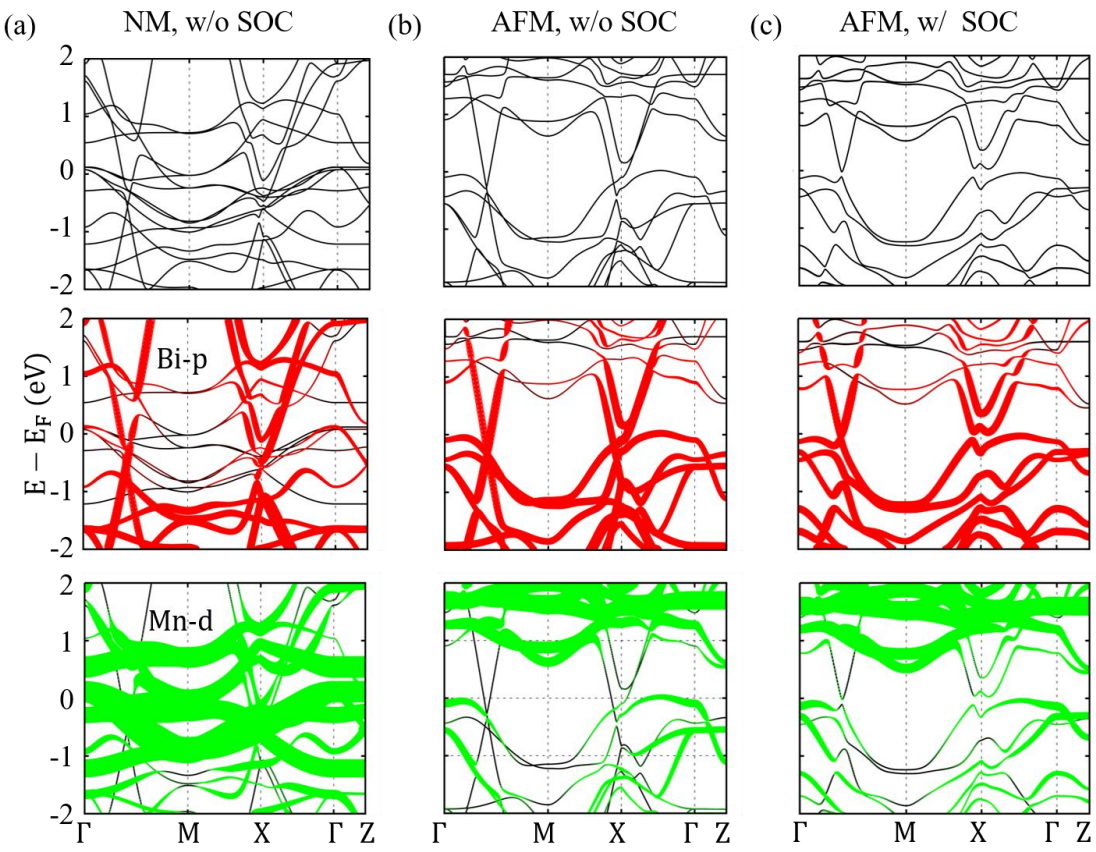

FIG. S4. DFT-calculated band structures of $SrMnBi_2$ under pressure and their projection onto Bi-*p* (red) and Mn-*d* (green) orbitals for (a) nonmagnetic (NM) and without SOC, (b) antiferromagnetic (AFM) and without SOC, and (c) AFM and with SOC.

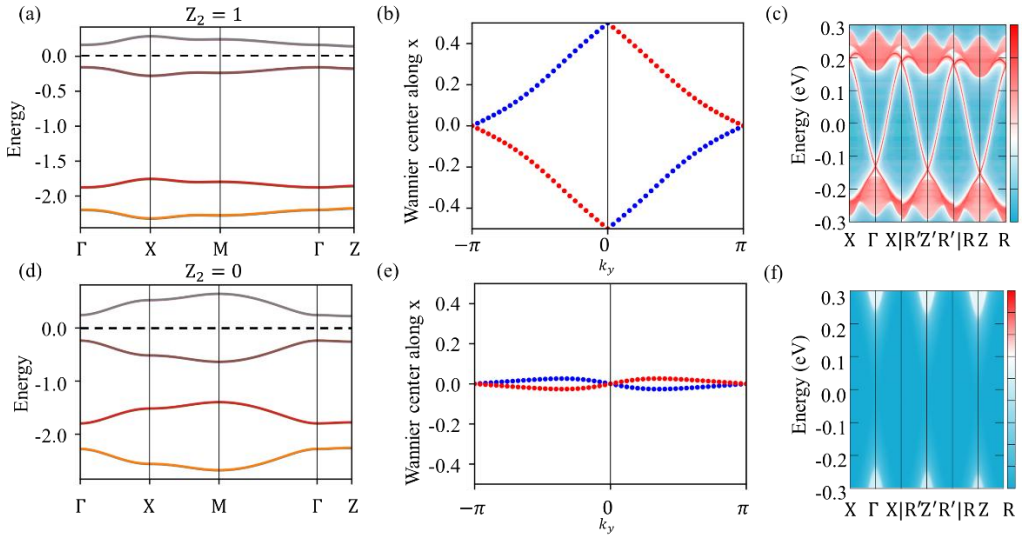

FIG. S5. Characterization of Z_2 phases protected by spin group symmetry. (a-c) energy band, Wilson loop at $k_z = 0$ plane and surface states for the topological nontrivial phase with the parameters of Eq. (S73) chosen as $(t, t', t_\perp, \Delta) = (0.1, 0.05, 0.1, 0.04)$ and $\boldsymbol{S_1} = -\boldsymbol{S_2} = (0, 0, -1)$. Red and blue curves in (b) show Wilson loops projected on two subspaces that are connected by $\{T||m_z|0\}$ symmetry. (d-f) Same as (a-c) but for the topologically trivial phase with the parameters of Eq. (S73) chosen as $(t, t', t_\perp, \Delta) = (0.1, 0.05, 0.1, 0.44)$ and $\boldsymbol{S_1} = -\boldsymbol{S_2} = (0, 0, -1)$.

References

[1] D. S. Dummit and R. M. Foote, *Abstract Algebra* (Wiley Hoboken, 2004), Vol. 3.

[2] H. Bethe, *Termaufspaltung in Kristallen*, Ann. Phys. (Berl.) **395**, 133 (1929).

[3] W. Opechowski, *Sur Les Groupes Cristallographiques "Doubles"*, Physica **7**, 552 (1940).

[4] Y. Yao, F. Ye, X.-L. Qi, S.-C. Zhang, and Z. Fang, *Spin-Orbit Gap of Graphene: First-Principles Calculations*, Phys. Rev. B **75**, 041401 (2007).

[5] J. Zak, *Band Representations of Space Groups*, Phys. Rev. B **26**, 3010 (1982).

[6] Y. Xu, L. Elcoro, Z.-D. Song, B. J. Wieder, M. G. Vergniory, N. Regnault, Y. Chen, C. Felser, and B. A. Bernevig, *High-Throughput Calculations of Magnetic Topological Materials*, Nature **586**, 702 (2020).

[7] L. Elcoro, B. J. Wieder, Z. Song, Y. Xu, B. Bradlyn, and B. A. Bernevig, *Magnetic Topological Quantum Chemistry*, Nat. Commun. **12**, 5965 (2021).

[8] P. Delplace, J. Li, and D. Carpentier, *Topological Weyl Semi-Metal from a Lattice Model*, EPL **97**, 67004 (2012).

[9] G. Lee, M. A. Farhan, J. S. Kim, and J. H. Shim, *Anisotropic Dirac Electronic Structures of AMnBi2 (A= Sr, Ca)*, Phys. Rev. B **87**, 245104 (2013).

[10] Z. Song, T. Zhang, and C. Fang, *Diagnosis for Nonmagnetic Topological Semimetals in the Absence of Spin-Orbital Coupling*, Phys. Rev. X **8**, 031069 (2018).